MODELING GROWTH OF *CHLORELLA SOROKINIANA* BY CHANGING CO_2 NUTRIENT CONCENTRATION AND PH DYNAMICS BY CONVECTIVE MASS TRANSFER

by

Nikolas Gruber

A Thesis Submitted to the Faculty of the

DEPARTMENT OF CHEMICAL AND
ENVIRONMENTAL ENGINEERING

In Partial Fulfillment of the Requirements for
the Degree of

MASTER OF SCIENCE

In the Graduate College

THE UNIVERSITY OF ARIZONA

2025

THE UNIVERSITY OF ARIZONA
GRADUATE COLLEGE

As members of the Master's Committee, we certify that we have read the thesis prepared by NIKOLAS GRUBER, titled MODELING GROWTH OF *CHLORELLA SOROKINIANA* BY CHANGING CO_2 NUTRIENT CONCENTRATION AND PH DYNAMICS BY CONVECTIVE MASS TRANSFER and recommend that it be accepted as fulfilling the thesis requirement for the Master's Degree.

KIMBERLY OGDEN Date: 4/23/25

AVELINO EDUARDO SAEZ Date: 4-23-25

PAUL BLOWERS Date: 4-23-25

Final approval and acceptance of this thesis is contingent upon the candidate's submission of the final copies of the thesis to the Graduate College.

We hereby certify that we have read this thesis prepared under our direction and recommend that it be accepted as fulfilling the Master's requirement.

KIMBERLY OGDEN Date: 4/23/25
Master's Thesis Committee Co-Chair
Chemical and Environmental Engineering

AVELINO EDUARDO SAEZ Date: 4-23-25
Master's Thesis Committee Co-Chair
Chemical and Environmental Engineering

ACKNOWLEDGEMENT

Thank you to everyone that helped me during this process.

Thank you to my family and friends for supporting me, believing in me, and offering me reprieve when it became necessary. Thank you for sticking with me through this.

Thank you to Dr. Kim Ogden and Dr. Saez for providing direction on my time in the lab, and Dr. Greg Ogden for setting up the systems I needed.

Thank you to my lab group who were always there to help me with my experiments and preparation.

Thank you to all my professors during my time here at U of A.

Table of Contents

Abstract

Changing pH in a system will have effects on almost all aspects of biological life in that system. Understanding how the pH changes in a system through the addition of CO_2 over time is important to determine how life in that system will react. Additionally, algae has been well-researched due to its potential in biofuel production and water treatment. Understanding the role of carbon dioxide availability on the growth of algae is important to produce enough algae for these uses. This study explores both the modeling of dynamic pH effects through use of the convective mass transfer coefficient and the growth effects of CO_2 on *Chlorella sorokiniana*. All algal growth experiments were conducted at a temperature of around 35° C, a light intensity of 234 μmol m^{-2} s^{-1}, and a 12-hour light phase in a 24-hour cycle. Experiments were conducted with feed CO_2 compositions between the concentration in air and 5%. A one parameter model was applied to data to find the growth rate. The trials showed that an excess composition of CO_2 does not have a significant impact on the growth rate while CO_2 limited trials give a decreased growth rate. The dynamic pH trials in different media were fit to a one parameter model. These pH experiments showed that the pH could be accurately modeled through the equations in this study and that the convective mass transfer coefficients for the absorption and desorption processes of CO_2 were likely different.

1. Introduction:

Global warming is an issue of increasing importance around the world. It is caused by greenhouse gas emissions into the atmosphere. The most common greenhouse gas is carbon dioxide (CO_2). These greenhouse gases trap heat in the atmosphere and warm the planet [1]. Global warming impacts many factors of life on earth, including but not limited to the environment and global population health [2].

These impacts have led to a global effort to find solutions to greenhouse gas emissions. The most well-known measure to address the problem is to minimize reliance on fossil fuels. This requires harvesting energy from renewable sources such as wind and solar. Another possible renewable energy source is using biofuel in lieu of petroleum [3]. Biofuel made from algae will help mitigate the amount of CO_2 released into the atmosphere.

The University of Arizona is working on a collaborative project with Tucson Electric Power, Lawrence Livermore National Laboratory (LLNL), Sandia NL, and Southwest Technologies to use algae to capture CO_2 from flue gas. The chosen strain of algae in this project is *Chlorella sorokiniana*, which converts CO_2 to biomass. The algae can then be repurposed for other uses such as biofuels or water treatment. The University of Arizona, where this study is conducted, has been tasked with fitting this algal growth to a model.

This growth will then be compared to growth while using a sorbent developed by LLNL. This sorbent was developed to more effectively transport and deliver inorganic carbon to algae for growth. The sorbent can capture CO_2 as sodium bicarbonate using a CO_2-permeable polymer. The sorbent can then be used to deliver CO_2 and control pH in algal cultures of up to 100 L [4]. Comparing the growth between the bubbling of the CO_2 and the sorbent-released CO_2 will aid in determining the ideal load of CO_2 in the sorbent and the optimal release.

This work aims to find the composition of feed gas where CO_2 becomes limiting to the algae growth as well as any effects of excess CO_2 on the growth. This was done through experiments where gas of varying CO_2 compositions was bubbled through a media solution with algae and the growth was measured over time. This work presents a dynamic pH model that was developed and to obtain the same volumetric convective mass transfer coefficient for both the absorption and desorption of the CO_2 in the media. This was done through the bubbling of gas with different CO_2 compositions through different media to find how the pH changes over time. This was done without algae in the system but can hopefully be extended to modelling the pH in a system with algae because pH affects virtually every

aspect of biological life [5].

2. Literature Review:

2.1 Dynamic pH Models

There are many circumstances in which dynamic pH changes affect the growth and development of biological life [5]. Modelling pH is a complex undertaking due to the large number of factors that influence it [6]. These factors include – but are not limited to – total inorganic carbon, total alkalinity, and cellular growth and respiration. Modelling the pH of an aqueous system has been found to be both a chemical equilibrium problem and a kinetic problem [7]. The significant differences in the time scales of these kinetic rates lead to the necessity of a stiff equation system solver. There are ways to reduce the stiffness of this system by employing higher-order non-linear complexity [6].

One of the main issues of modeling pH dynamics is the diversity of approaches and the lack of cross-linking between the methods [6]. This leads to difficulties in assessing the accuracy and replicability of the models. A second issue stems from the complexity inherent in the model. The process of modelling the dynamic pH can be simplified if done in an aqueous system without presence of biological cells. This eliminates the inherent uncertainty of biological processes and growth and the effects on the system [8]. This allows for modeling using fluxes as well as chemical equilibrium equations. When CO_2 is bubbled through an aqueous solution (open system), the equilibrium equations of relevance are shown in Equations L1-L3.

$$CO_{2(aq)} + H_2O \rightleftharpoons H_2CO_3 \quad (L1)$$

$$H_2CO_3^* \rightleftharpoons H^+ + HCO_3^- \quad (L2)$$

$$HCO_3^- \rightleftharpoons H^+ + CO_3^= \quad (L3)$$

A pseudo-species [$H_2CO_3^*$] can be used to represent the sum of [H_2CO_3] and [$CO_{2(aq)}$] present in the system and is usually present in negligible concentrations. This means that [$H_2CO_3^*$] can be represented by Henry's Law. This and the equilibrium relations of importance can be represented by Equations L4-L7. K_H, K_{a1}, and K_{a2} are from literature [9] at 25ºC and values of $10^{-1.47}$ mol/Latm, $10^{-6.35}$, and $10^{-10.33}$, respectively

$$[H_2CO_3^*] = [H_2CO_3] + [CO_{2(aq)}] \quad (L4)$$

$$[H_2CO_3^*] = K_H P_{CO_2} \quad (L5)$$

$$K_{a1} = \frac{[H^+][HCO_3^-]}{[H_2CO_3^*]} \quad (L6)$$

$$K_{a2} = \frac{[H^+][CO_3^{=}]}{[HCO_3^-]} \quad \text{(L7)}$$

2.2 Convective Mass Transfer

Convective mass transfer is the transport of mass between surfaces and moving fluids and is driven by both bulk fluid motion and molecular diffusion [10]. When bubbling gas through an aqueous solution, it is appropriate to use convective mass transfer to represent the transfer of CO_2 between phases [11]. The change in the total CO_2 concentration in the liquid can be expressed by Equation L9. In this equation, c_T represents the total molar concentration of CO_2 present in the system and k_ca represents the volumetric mass transfer coefficient [Appendix A]. These are shown in Equations L8 and L9.

$$c_T = [H_2CO_3^*] + [HCO_3^-] + [CO_3^{=}] \quad \text{(L8)}$$

$$\frac{dc_T}{dt} = k_c a(K_H P_{CO_2} - [H_2CO_3^*]) \quad \text{(L9)}$$

The convective mass transfer coefficient k_c can be difficult to isolate from a because a represents the surface area of the gas bubbles in the system per unit volume of the liquid. Often, these can be difficult to measure due to the actual bubble geometry, velocity, and nature of the setup of the system (Mondal). It is much simpler to represent k_ca as a single parameter in a model. This parameter is called the volumetric convective mass transfer coefficient.

For a system with a given P_{CO_2}, Equations L5-L8 and L10 can be used to calculate a predicted equilibrium pH and the concentrations of all species at this point. In the case that the P_{CO_2} is unknown or uncertain, these equations can be used with an experimentally obtained equilibrium pH to find a P_{CO_2} value.

A previous study found that volumetric convective mass transfer coefficients of a gas bubbled through an aqueous solution are generally on the order of 0.3 min^{-1} to 3 min^{-1}. This study pulled data from many previous studies to give this range [12]. This gives a wide range of possible values, but can be then used to compare results using a variety of gases in aqueous medias.

2.3 Buffering and Charge Balances

Buffering within an aqueous system is a method of resisting changes to pH from the addition of external factors. This is done using a solution of known pH or introducing factors to influence the pH in a

known manner [13]. This pH is known in a system through use of the charge balance, which makes sure that the positive and negative charges within a system are equal. For the addition of CO_2 in distilled water the charge balance can be represented by Equation L10.

$$[H^+] = [HCO_3^-] + 2[CO_3^=] + [OH^-] \quad \text{(L10)}$$

There have been studies that model the pH of a system through the minimization of the charge balance by iteration until both sides are equal. These studies use a similar charge balance to find the concentration of hydrogen ions, which can be related directly to pH. The study used this charge balance to find and model the interactions between acids and bases when making use of ionic activity coefficients [14].

2.4 Algal Growth

Algae are photosynthetic organisms that serve as oxygen producers and are the base food source for almost all aquatic life [15]. This means that algae are very important to all life. Algae require light, carbon dioxide, and additional nutrients to grow [16]. The key to optimizing algae growth is the optimization of these conditions. There have been many studies about these conditions. Many of these studies attempted to create combinations of these factors in which specific strains of algae could grow optimally. It was found that light wavelength has a noticeable effect on algal growth and that blue and clear light were more conducive to growth than red and green light [17]. It was also found that light intensity and temperature impact the growth of *Chlorella sorokiniana* in a study that also used a BioFlo reactor [18]. That study found that the optimal light intensity for algal growth was 234 μmol m^{-2} sec^{-1} but could result in possible photooxidation due to clumping and settling of the algae. This study also found that the algae was very sensitive to temperature, and that the optimal temperature for growth was around 32º-35º C.

In a previous study, it was found that *Chlorella sorokiniana* growth rates were around 1 day^{-1} to 5 day^{-1}. This was found using a one-parameter light intensity growth model [19]. This study was able to effectively model the growth rate of algae as a function of light intensity. A separate study found that the maximum growth rate for *Chlorella sorokiniana* occurred at a pH of 7, whereas the maximum overall growth occurred at a pH of around 6, generally decreasing as pH increased. This study also concluded that growth at a pH of 8 was most cost-effective by using the least CO_2 per gram of algae [20].

In addition to light and temperature, carbon dioxide availability and nutrient availability also

affect algae growth. Nutrient availability varies based on the chosen media but typically includes some combination of nitrogen and carbonate [21]. The components of the media that contribute most to growth will depend on the strain of algae used for the experiment [22]. An increase in carbon dioxide availability generally increases the growth in algae but will result in poisoning the algae if too high [23]. This shows that there is an optimal CO_2 concentration for algal growth and that CO_2 availability can be a limiting factor in growing algae.

2.5 Algal Models

Accurately modeling algal growth can be difficult [24]. There are many factors that affect growth, which makes creating a model that accounts for all factors difficult. As a result, many different algal growth models exist. Many of these can be split into the categories of temperature and light dependent or nutrient dependent. Different models are better for different strains of algae. Additionally, different models are used depending on the conditions of algal growth. For example, when nutrients are in abundance, light availability and temperature are the limiting factors on the growth and will need to be accounted for in the chosen model. In light and temperature-controlled experiments, nutrient based models will need to be used.

For the algae to grow optimally, there must be a dark phase and a light phase in the growth cycle of the algae [25]. Too little light availability leads to a light-limited growth curve and too much light will cause photooxidation, which decreases growth rate. At ideal temperature and light conditions, the growth is dependent on the availability of nutrients. These nutrients include nitrogen, phosphorus, and carbon [26].

2.6 Algae Applications

Algae can be utilized for many applications. Among these applications are renewable biofuel, nutrition, and wastewater treatment. Algae use as renewable biofuel is important because it can replace a nonrenewable source like petroleum. Petroleum has been used for centuries, and the use has been increasing. Replacing much of this use with algae biofuel is a more sustainable model and reduces greenhouse gas emissions [3].

Nutritionally, algae can be used to help support the increasing global need for dietary protein. Algae is abundant and environmentally sustainable, as well as being a good source of protein. Consuming algae has been shown to protect glucose and lipid homeostasis and have anti-inflammatory properties

[27]. Bioactive compounds such as phycobiliprotein and carotenoids can also be extracted from algae for use in medicine [28].

Algae can also be used to treat wastewater and other water sources. Due to their capacity to remove heavy metals and some toxic organic compounds, the addition of microalgae in the wastewater treatment process can be important [29]. With the rising prevalence of microplastics as pollutants, it is also important to note that algae is able to remove some microplastics from the water supply [30]. Microplastics are toxic and pose risks to many ecosystems. They also can cause DNA damage and organ dysfunction in humans [31]. For these reasons, algae can be a beneficial additive to the water supply.

2.7 Review Conclusion

Note: Review Conclusion written with help from ChatGPT

This literature review highlights the complex interplay between chemical, physical, and biological factors in dynamic pH modeling, convective mass transfer, buffering systems, and algal growth. Accurately modeling pH in aqueous systems requires consideration of both equilibrium and kinetic processes, with significant challenges arising from system stiffness and model complexity. Simplifying these models through assumptions – such as excluding biological components – can improve tractability but may limit applicability of the model.

Convective mass transfer plays a critical role in systems involving CO_2 diffusion, and its accurate representation is essential for modeling carbon availability in algal cultures. Buffering and charge balance principles are key to maintaining system stability and are commonly used to relate ionic species to pH. Algal growth models further complicate the system due to the sensitivity of algae to light, temperature, nutrients, and CO_2 levels, all of which must be carefully optimized for both experimental and industrial applications.

Together, these studies underscore the necessity for integrated modeling approaches that can account for the dynamic and interdependent nature of aqueous systems involving algae. Understanding and improving these models is not only vital for advancing biofuel technologies and water treatment methods but also for supporting sustainable biological systems in the face of environmental change.

3. Methodology:

3.1 Algae Strain

All experiments were run using the *Chlorella sorokiniana* DOE1412, a member of the Trebouxiophyceae class, also known as UTEX B 3016. This strain is well-researched and often used in experimentation [32]. *Chlorella sorokiniana* is a strain of algae that has been shown to grow well in inorganic media [33]. Additionally, the species has been shown to have good light-use efficiency [34]. It also has large nutritional and biofuel potential [32]. For these reasons, *Chlorella sorokiniana* was used as the strain of algae for these experiments.

3.2 Media

All experiments were performed using 2 L of PECOS media. The ingredients and equipment must be autoclaved prior to use. The recipe for the media can be found in Table 3.1. The balance of the media was autoclaved distilled water that had cooled.

Table 3.1-PECOS Media

PECOS media on a 2-liter total basis

Chemical	Final concentration (g/L)	Stock Solution Concentration (g/L)	Volume (mL)
$(NH_2)_2CO$ (urea)	0.1	20	10
$MgSO_4$*7H2O	0.012	12	2
$NH_4H_2PO_4$	0.025	25	2
Potash	0.075	37.5	4
$FeCl_3$	0.00315	3.15	2
Na_2CO_3	0.02	20	2
EDTA	0.00436	1.09	8
Allens solution	/	/	2

Table 3.2-Allens solution

Per 1 liter basis

Chemical	Amount (g/L)	Final Concentration (µM)
H_3BO_3	2.86	46
$MnCl_2$*4H2O	1.81	9
$ZnSO_4$*7H2O	0.22	0.77
Na_2MoO_4*2H2O	0.39	1.6
$CuSO_4$*5H2O	0.079	0.3
$Co(NO_3)_2$*6H2O	49.4	0.17

3.3 Piping and Instrumentation Diagram (PID)

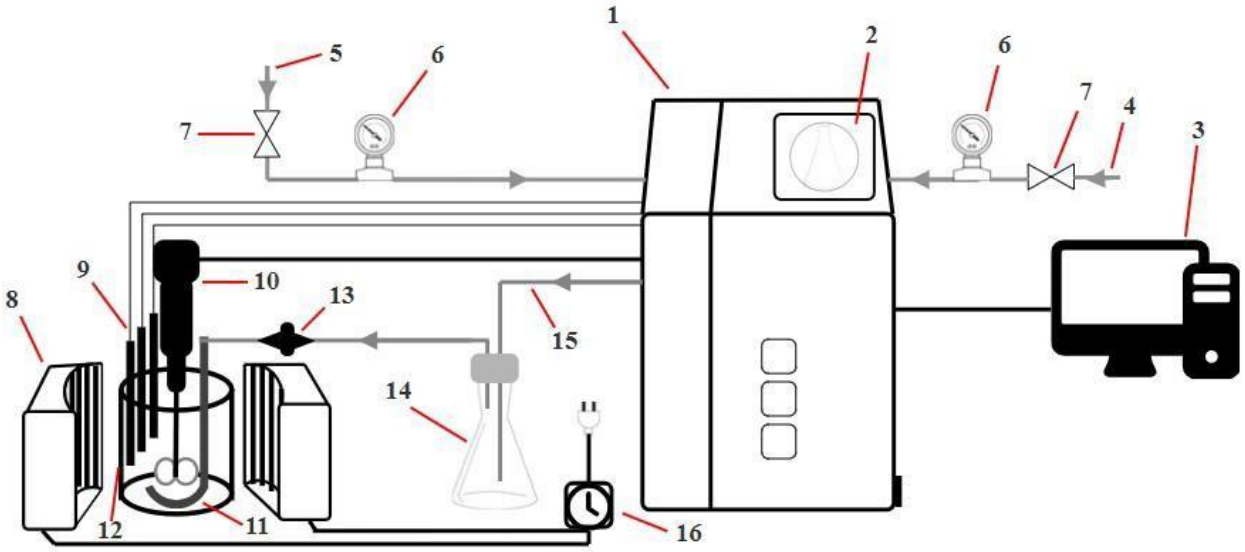

Figure 3.1: PID of full reactor setup

1	BioFlo 115 controller/computer
2	BioFlo interface
3	Desktop PC with BioFlo program and data storer
4	Air gas line
5	CO_2 gas line

6	Pressure gauge/regulator
7	Gas on/off valve
8	Light units
9	DO, pH, and temperature probes
10	Agitation motor
11	Gas bubble diffusor
12	Batch reactor
13	Gas particle filter
14	1L Erlenmeyer flask filled with 500ml water
15	Mixed gas reactor inlet
16	Lights timer

A schematic of the bioreactor is shown in Figure 3.1. The reactor is the New Brunswick model of the BioFlo/CellGen 115 system from Eppendorf. This system allows for up to four gases to be mixed and fed to the reactor. The gases are split by percentage and controlled by opening internal gas valves for varying amounts of time. The gas is then internally mixed before being fed to the reactor. [35] The BioFlo is connected to pH, temperature, and dissolved oxygen probes that collect dynamic data from within the reactor. The data was collected using the corresponding BioCommand Track and Trend software on the desktop PC.

Experiments were run setting the feed gas compositions of CO2 to 5%, 3.5%, 1.8%, 0.8%, 0.3%, and 0.15% in air by volume. An additional experiment was run with 0% CO2 as a control. All runs were fed a total flow rate of gas of 2 SLPM, received 12 hours of light per day, and were agitated with the motor at a rate of 125 RPM to prevent settling.

3.4 Reactor Setup/Takedown

At the conclusion of each run, the reactor was cleaned and set up in preparation of the next experiment. To do this, agitation and gas flow were turned off and the probes and gas line were removed. The algae solution was killed with a bleach and poured down the sink. The reactor was washed by hand with soap, rinsed, and autoclaved. The DO and pH probes were rinsed with distilled water and the pH probe was stored in pH 7 solution between experiments.

To begin the next experiment, PECOS media was prepared and added to the reactor. The probes were reinserted after calibration and the gas line was reconnected. The settings for the new run were then set and a new inoculum of algae was added such that the initial OD readings were just over 0.1.

3.5 Cell Growth Measurements

Optical density (OD) readings were taken at wavelengths of 650 nm and 780 nm using a Genesys 10S UV-Vis spectrophotometer from Thermo Scientific. Both 650 nm and the 780 nm can be used to find the cell concentration. However, the 650 nm wavelength also can be affected by the chlorophyl content, or "greenness" of the sample while the 780 nm wavelength can be directly related to the cell concentration through ash free dry weight [36].

Measurements were performed by taking a 5-10 mL sample of the algae in media using a 10 mL pipette. The spectrophotometer was blanked with distilled water and 1 mL of the algae sample was measured into each of three cuvettes and ran through the spectrophotometer. Three optical densities are taken for increased accuracy and averaged to get a data point where the time of sampling was also recorded.

Due to inaccuracies in the spectrophotometer, the samples had to be diluted when an optical density higher than 1 was read. This was done by changing the 1 mL algae samples to 900 µL distilled water and 100 µL algae. This gave an optical density reading that was multiplied by 10 to get the actual data.

3.6 Ash Free Dry Weight

Ash free dry weight is a procedure used to match the OD readings to a mass concentration of algae. This was performed with the readings at 780 nm as the independent variable because those correspond to cell density.

The process of ash free dry weight (AFDW) begins with Whatman Grade GF/C filters with fine nominal particle retention of 1.2 µm. The filter is rinsed utilizing distilled water and a vacuum system. The filter was then pre-ashed in a muffle furnace for 4 hours at 540°C. The filter was then weighed.

The optical density readings of the algae were taken and then 20 mL of the algae was added to the filter in the vacuum system. The vacuum was run until there was no longer liquid draining through the filter. The filter with algae was then placed for 2 days in an oven at 105°C to fully dry the algae.

The filter is weighed again to determine how much algae mass was in 20 mL of the solution. The filter is put again into the muffle furnace at 540°C for 4 hours. The filter is then weighed for the ash content of the 20 mL of algae. From this, the amount of algae in the 20 mL sample can be determined. This can then be graphed against optical density to determine a correlation. Once the line of best fit is created, all data from the experiments can be transformed from OD to ash free dry weight values.

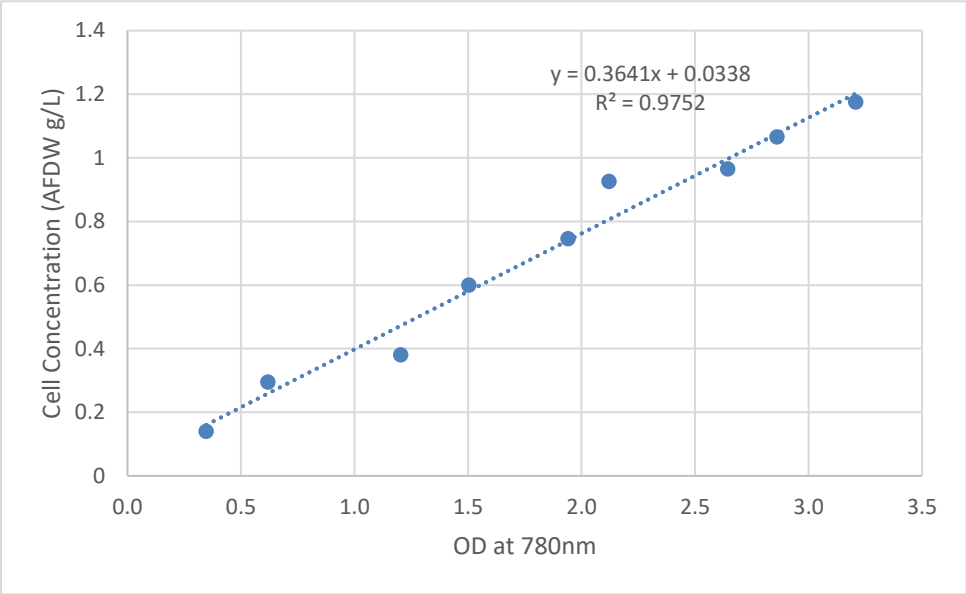

Figure 3.2: Ash free dry weight of Chlorella sorokiniana fit to wavelength 780nm

3.7 General Maintenance

The gas cylinder supplying CO_2 was replaced when the observed pressure of the cylinder reached 0 to ensure a consistent feed of CO_2 to the reactor. The pressure of the gas line feed to the reactor was set and maintained at 10 psi for all experiments.

The CO_2 supply was integral to the operation of the experiment and thus could not be out for more than 4 hours during the light phase of the cycle or the experiment would need to be restarted. The CO_2 levels were checked at the time of OD readings.

During experiments, it was important to minimize the amount of evaporation from within the reactor. This was addressed by first bubbling the inlet gas through distilled water in the Erlenmeyer flask so it was saturated before coming in contact with the algae solution. When the water level in the flask got too low to bubble through, more distilled water was added.

For all experiments, it was necessary to maintain a reactor volume of 2 L to ensure the accuracy of the model. When the level dipped below 2 L, distilled water was added to the reactor to maintain the 2 L volume.

3.8 Calibration of Probes and Sensors

After each experiment, it was necessary to recalibrate the pH and dissolved oxygen (DO) probes due to possible drift to minimize the possibility of inaccuracies. The pH probe was rinsed thoroughly with distilled water in order to remove any residues or contaminants. The probe was then held by a clamp in standards of pH 4, 7, and 10 with rinsing repeated in between. The clamp was used to ensure that the probe was steady and did not touch the walls of the bottle of standard.

The probe readings were allowed to stabilize in each standard before the point was set using the BioFlo computer. Two ranges were used to calibrate the probe, one being a pH of 4-7 and the other as 7-10.

Similarly to the pH probe, the DO probe was rinsed thoroughly with distilled water in order to remove any residues or contaminants after each experiment. To calibrate the probe to 0, the probe was briefly disconnected from the BioFlo computer and set prior to being reattached. To calibrate the DO probe to 100, flush the reactor filled with media with air and set 100 when the readings are level.

3.9 Algae Growth Model

The model used to fit the experimental growth data uses Verhulst kinetics [37], where X represents the algae concentration, X_M represents the maximum concentration of algae achieved with full growth, and μ represents the growth rate. This is shown in Equation 1.

$$\frac{dX}{dt} = \mu X\left(1 - \frac{X}{X_M}\right) \quad (1)$$

The growth rate μ is a function of all factors that influence the growth rate, such as CO_2 feed concentration, light availability and intensity, nutrient concentrations, temperature, and the presence of any inhibitors. In these experiments, μ could be considered constant leading to an integrated form of the Verhulst kinetic equation. This integrated equation is shown in Equation 2, with the initial concentration of algae denoted as X_0.

$$X = \frac{X_0 X_M e^{\mu t}}{X_M - X_0(1 - e^{\mu t})} \quad (2)$$

In the use of this model for these experiments it was assumed that the algae would neither grow nor die during the 12-hour dark phase daily to simplify the calculations. As a result, the model was paused during this dark phase and only showed growth during the 12-hour light phase. The initial and maximum concentrations were obtained from the data. Each experiment began with a 6-hour light phase for consistency.

Growth was modeled in Excel and solver was used to find the μ that made the model best fit the experimental data. The best fit was determined utilizing a least squares regression, quantified by the regression coefficient *r*. In Equation 3, y_i represents the i-th observed value of concentration from the data, $\hat{y}_i$ represents the i-th predicted concentration from the model, and $\bar{y}$ represents the average observed concentration over all data points.

$$r^2 = 1 - \frac{\sum(y_i - \hat{y}_i)^2}{\sum(y_i - \bar{y})^2} \quad (3)$$

3.10 Dynamic pH Experiments

Experiments were performed to model pH changes with time when introducing CO_2 into the PECOS media without algae. The same procedure was used as was when starting an algae growth experiment except lights were not included in the setup and algae was not added to the media.

The media was saturated with air by bubbling air through. When pH readings stopped changing with time, the CO_2 was introduced into the feed gas at a low percentage of 0.3%. The total flowrate was set to 2 SLPM throughout. A low percentage of CO_2 was chosen so that the equilibrium would take a substantive amount of time for to increase accuracy in modeling.

After the pH readings stopped changing with time, the flow of CO_2 was stopped and the media was again saturated with air, still set at the gas flowrate of 2 SLPM. After equilibrium pH was reached, data collection was stopped.

3.11 Dynamic pH Model

The model used to fit the data was based on CO_2 dissolution in aqueous media and the charge balance in PECOS media. The formation of the model is explained in Appendix A. A few key equations

are given in Equations 4-10.

$$K_{a1} = \frac{[H^+][HCO_3^-]}{[H_2CO_3^*]} \quad (4)$$

$$K_{a2} = \frac{[H^+][CO_3^=]}{[HCO_3^-]} \quad (5)$$

$$K_w = [H^+][OH^-] \quad (6)$$

Equilibrium constants K_{a1} and K_{a2}, as well the water dissociation constant K_W, were obtained from literature [9] at 25°C. The charge balance in PECOS media is shown in Equation 7.

$$[+] + [H^+] = [HCO_3^-] + 2[CO_3^=] + [OH^-] \quad (7)$$

[+] represents the sodium ion concentration in the PECOS media. Sodium was found to be the only ion affecting pH because of its bonding to carbonate and the dissolution of Na_2CO_3 in the aqueous media. At equilibrium, $[H_2CO_3^*]$ can be represented by Henry's Law as shown in Equation 8.

$$[H_2CO_3^*] = K_H P_{CO_2} \quad (8)$$

The Henry's Law constant at 25°C, K_H, was obtained from literature [9]. P_{CO_2} is set in the experiment. The total concentration of CO_2 in the liquid is given in Equation 9.

$$c_T = [H_2CO_3^*] + [HCO_3^-] + [CO_3^=] \quad (9)$$

This total CO_2 concentration can be modeled by Equation 10, where $k_c a$ represents a volumetric mass transfer coefficient formed from the mass transfer coefficient (k_c) and the specific surface area of gas bubbles (a).

$$\frac{dc_T}{dt} = k_c a(K_H P_{CO_2} - [H_2CO_3^*]) \quad (10)$$

The model was utilized to predict pH at all times in the experiment through the process described in Equations 11-26. This dynamic pH was modeled in Excel where solver was used to find the $k_c a$ that made the model best fit the experimental data.

Equilibrium points were found using this model by utilizing Equations 4-9 as well as the known constants and partial pressure of carbon dioxide. Equations 4-6 can be written as below, respectively, in terms of these known constants and $[H^+]$.

$$[HCO_3^-] = \frac{K_{a1}[H_2CO_3^*]}{[H^+]} = \frac{K_{a1}K_H P_{CO_2}}{[H^+]} \quad (11)$$

$$[CO_3^{=}] = \frac{K_{a2}[HCO_3^-]}{[H^+]} = \frac{K_{a1}K_{a2}K_H P_{CO_2}}{[H^+]^2} \quad (12)$$

$$[OH^-] = \frac{K_W}{[H^+]} \quad (13)$$

Utilizing Equations 11-13, the charge balance (Equation 7) can be rewritten as Equation 14.

$$[+] + [H^+] = \frac{K_{a1}K_H P_{CO_2}}{[H^+]} + 2\frac{K_{a1}K_{a2}K_H P_{CO_2}}{[H^+]^2} + \frac{K_w}{[H^+]} \quad (14)$$

Equation 9 can also be rewritten as Equation 15 by utilizing the equilibrium relationships given in Equations 8, 11, and 12.

$$c_T = K_H P_{CO_2} + \frac{K_{a1}K_H P_{CO_2}}{[H^+]} + \frac{K_{a1}K_{a2}K_H P_{CO_2}}{[H^+]^2} \quad (15)$$

Solver in Excel could then be used to find $[H^+]$ that satisfies Equation 11. This $[H^+]$ is subject to the realistic bounds of being a real, positive number. The equilibrium pH was then found through the well-known relation in Equation 16.

$$pH = -\log[H^+] \quad (16)$$

Many equilibrium points were found using this model. These points were plotted to find a relation between $[H_2CO_3^*]$ from Equation 8 and c_T from Equation 15. The plot for PECOS media is shown in Figure 3.3.

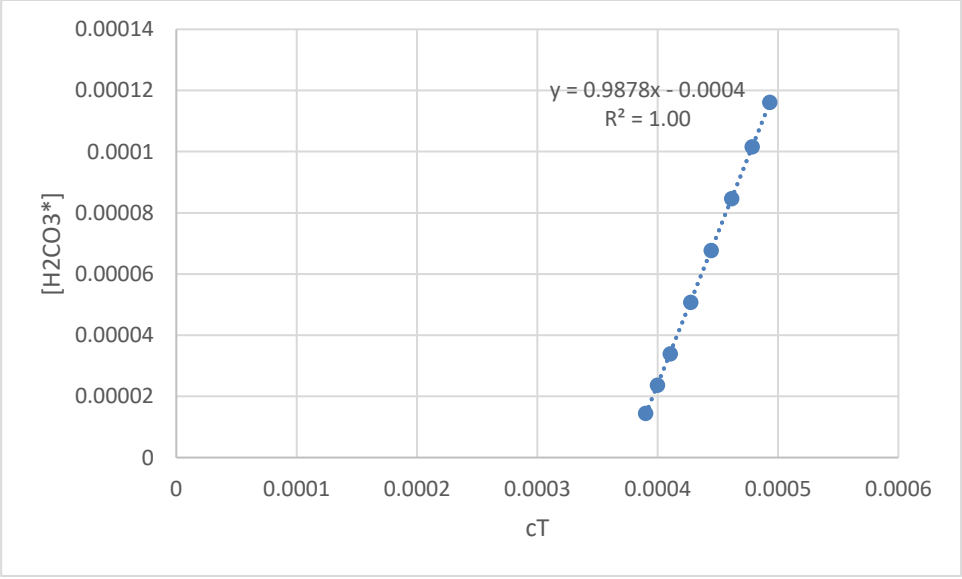

Figure 3.3: $[H_2CO_3^*]$ relation to c_T

This clearly results in a linear relationship between the two variables, meaning that $[H_2CO_3^*]$ can be rewritten in Equation 17, where *m* is the slope of the fit and *b* is the intercept. *m* and *b* were refit in Excel using solver for higher accuracy.

$$[\mathrm{H_2CO_3^*}] = mc_T + b \tag{17}$$

By plugging Equation 17 into Equation 10, Equation 10 can be rewritten as Equation 18.

$$\frac{\mathrm{dc_T}}{\mathrm{dt}} = \mathrm{k_c a}\left(\mathrm{K_H P_{CO_2}} - (mc_T + b)\right) \tag{18}$$

When solved for c_T, Equation 18 becomes Equation 19 below, where c_{T_0} represents the initial c_T value at the predicted initial equilibrium pH.

$$c_T = \left(c_{T_0} - \frac{K_H P_{CO_2} - b}{m}\right) e^{-k_c amt} + \frac{K_H P_{CO_2} - b}{m} \tag{19}$$

The model was then related to $[H^+]$ by recalling Equation 17, and the non-equilibrium parts of Equations 11 and 12. When plugging these equations into Equation 9, the result is Equation 20.

$$c_T = (\mathrm{mc_T} + b) + \frac{\mathrm{K_{a1}(mc_T} + b)}{[\mathrm{H^+}]} + \frac{\mathrm{K_{a1} K_{a2}(mc_T} + b)}{[\mathrm{H^+}]^2} \tag{20}$$

Equation 20 shows that $[H^+]$ can be written in quadratic form by rearranging and multiplying all terms by $[H^+]^2$.

$$((1 - \mathrm{m})c_T - b)[\mathrm{H^+}]^2 - \mathrm{K_{a1}(mc_T} + b)[\mathrm{H^+}] - \mathrm{K_{a1} K_{a2}(mc_T} + b) = 0 \tag{21}$$

Equation 21 can be solved for $[H^+]$ using the quadratic formula (shown below in Equation 25) as well as A, B, and C given below.

$$A = (1 - \mathrm{m})c_T - b \tag{22}$$

$$B = -\mathrm{K_{a1}(mc_T} + b) \tag{23}$$

$$C = -\mathrm{K_{a1} K_{a2}(mc_T} + b) \tag{24}$$

$$[\mathrm{H^+}] = \frac{-B \pm \sqrt{B^2 - 4AC}}{2A} \tag{25}$$

Subject to the constraints of $[H^+]$, only one root is left.

$$[\mathrm{H^+}] = \frac{-B + \sqrt{B^2 - 4AC}}{2A} \tag{26}$$

Equation 16 is then solved with the $[H^+]$ value obtained from Equation 26 and plotted as a data

point in the model. Dynamic pH was modeled in Excel and solver was used to find the $k_c a$ value that made the model best fit the experimental data. The best fit was determined utilizing a least squares regression shown in Equation 3. r^2 was maximized by changing $k_c a$.

4. Results and Discussion:

Modeling is important because models can help predict the outcome and behavior of experiments that have not, or cannot be, run. In the algae growth experiments, the growth was fit to a one parameter Verhulst kinetics model seen in Equation 2. In these experiments, the pH, DO, and temperature were also recorded over the duration of the growth. In the dynamic pH experiments, the change in the pH was fit to a one parameter mass transfer equation. This relation can be seen in Equations 4-26. These models could be used to further understand the processes they represent.

4.1 Algal Growth Results and Discussion

In the algal growth modeling, two replicate experiments were conducted using pure air as the feed gas. The air runs and their model fits can be seen in Figures 4.1 and 4.2. Both air runs resulted in very similar growth of the algae over time (seen in Figure 4.3) as well as very similar maximum concentrations and growth rate constants when fit with the model, which can be observed in Table 4.1. Due to these similarities, the two replicate air runs were combined, and the combination was modeled, as shown in Figure 4.3.

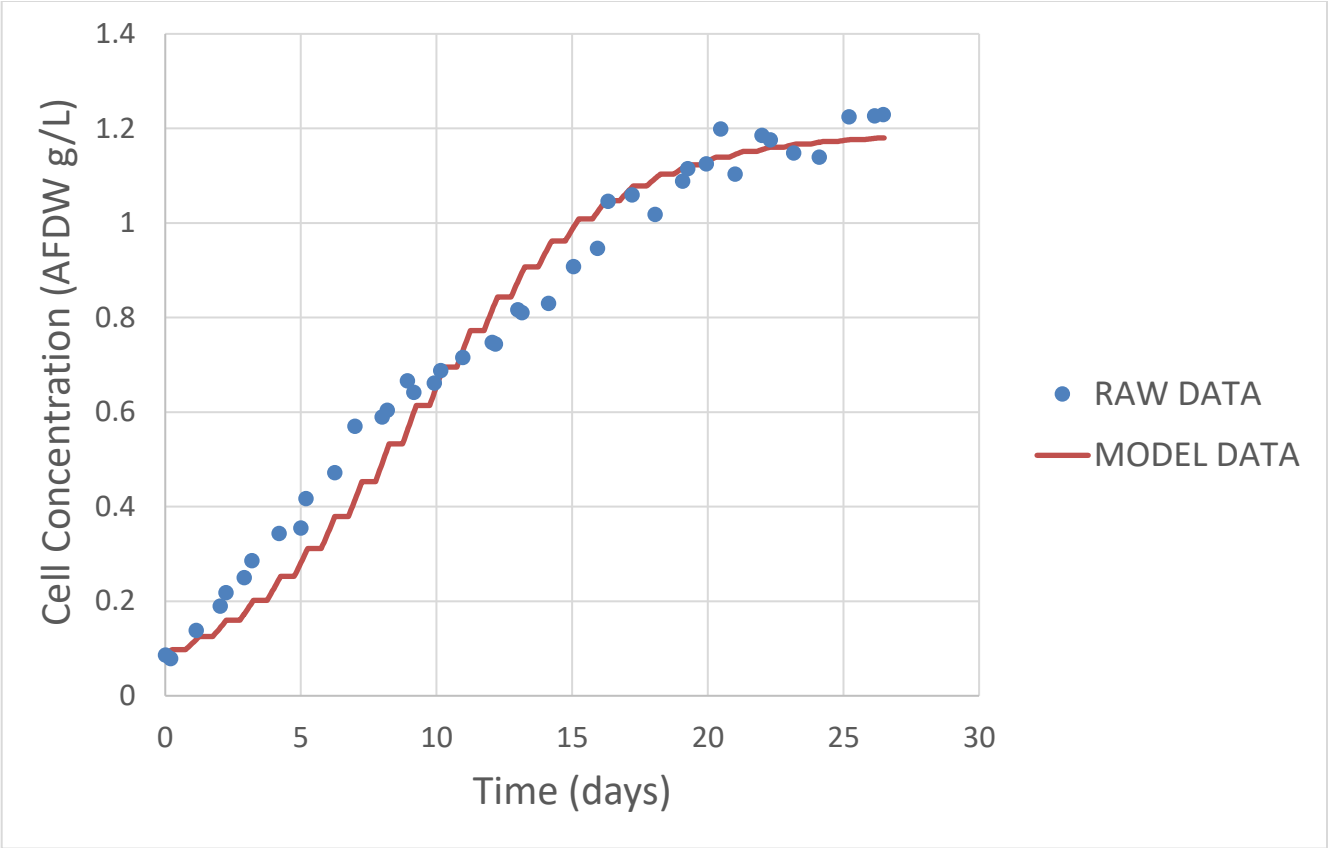

Figure 4.1: Chlorella sorokiniana growth in Air Trial 1 with a fit growth constant of 0.550 day^{-1} and an X_M of 1.19 g/L

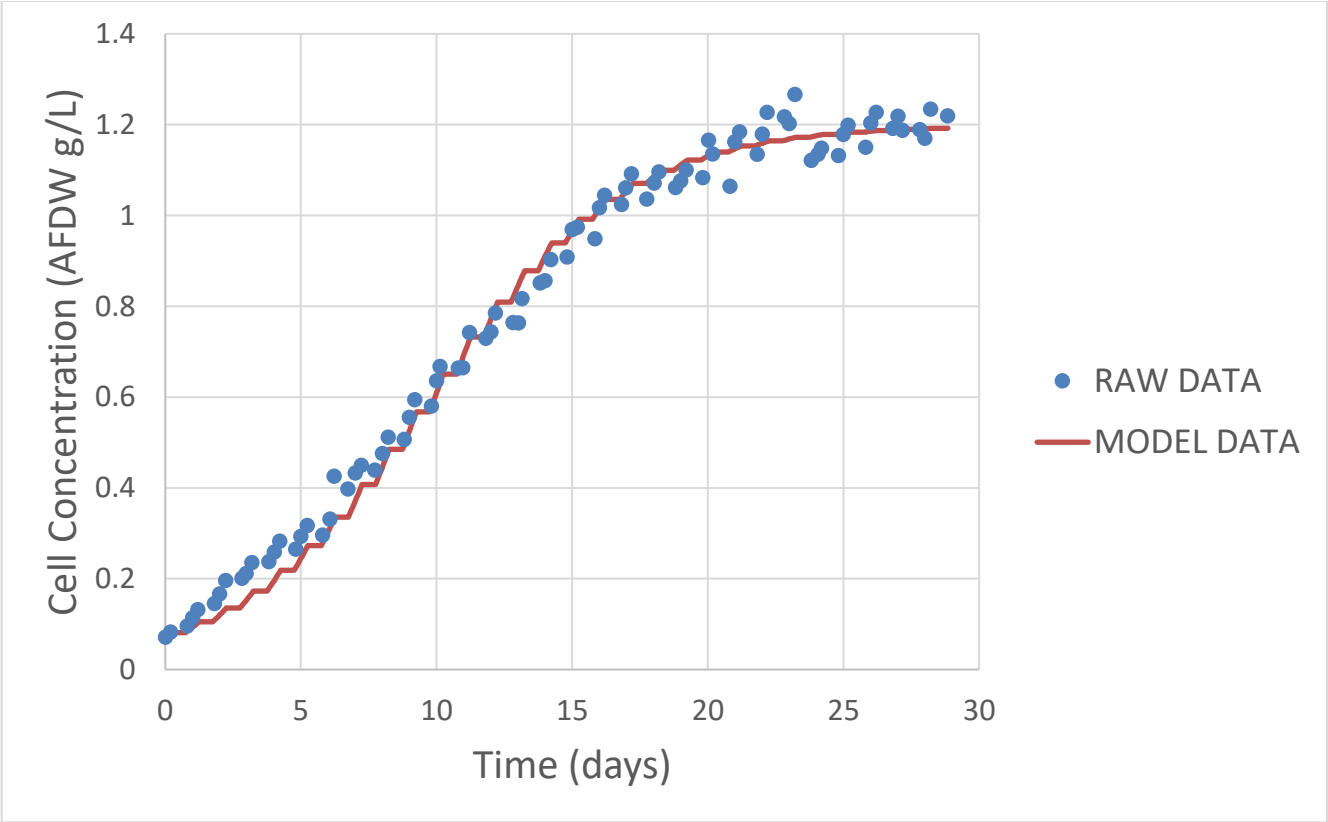

Figure 4.2: Chlorella sorokiniana growth in Air Trial 2 with a fit growth constant of 0.558 day^{-1} and an X_M of 1.120 g/L

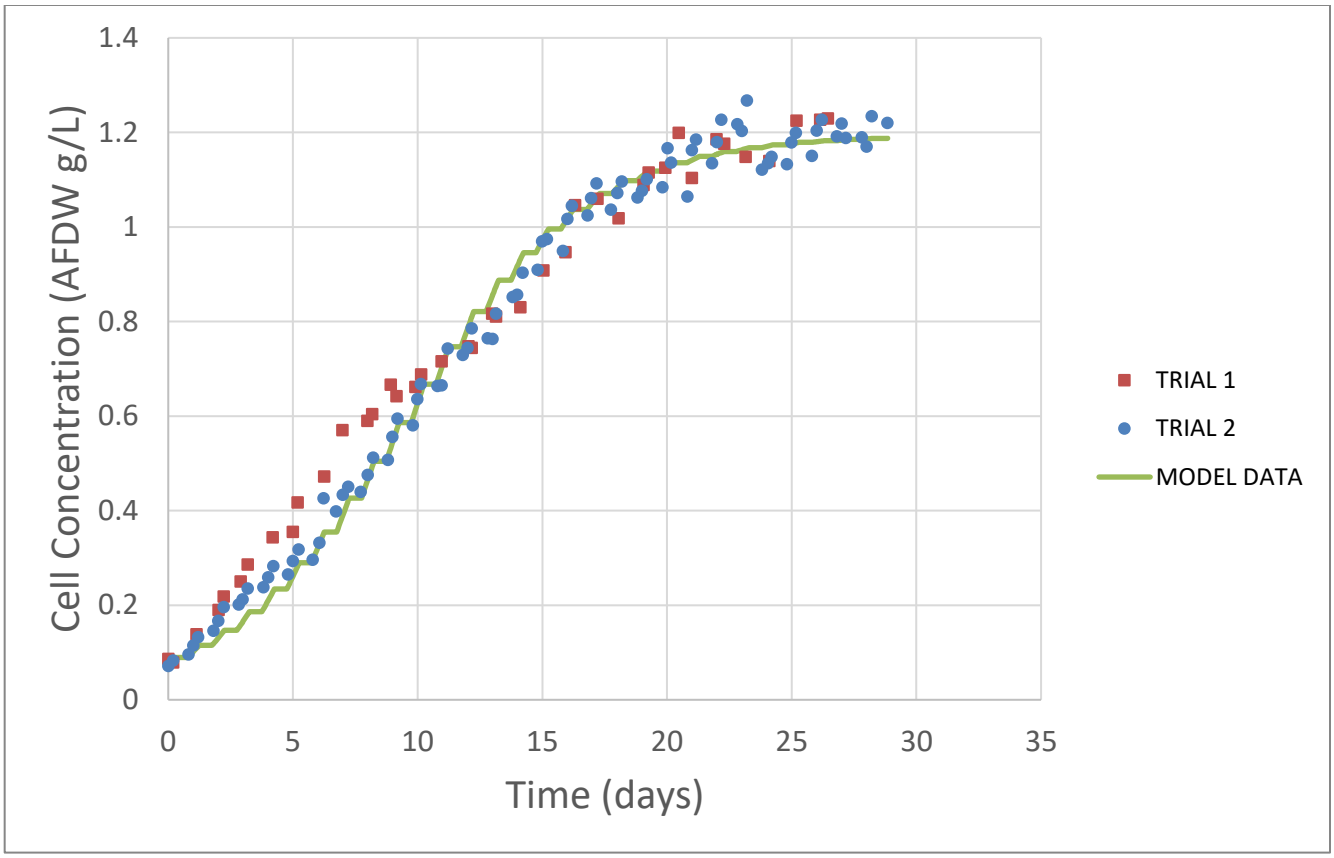

Figure 4.3: Chlorella sorokiniana growth in air trials with a combined fit growth constant of 0.550 day^{-1} and an X_M of 1.19 g/L

In addition to the similarities in the growth data between these two runs, the pH, DO, and temperature of these runs show minimal differences. These can be seen in Figures 4.4-4.6. Minor differences in the trends of the two runs exist but can be explained by slight difference in the calibration of the pH and DO probes, as well as a small variation in the surrounding temperature which may have been caused by a small movement of the light sources. The DO probe was likely not properly calibrated prior to trial 2, resulting in the observed difference.

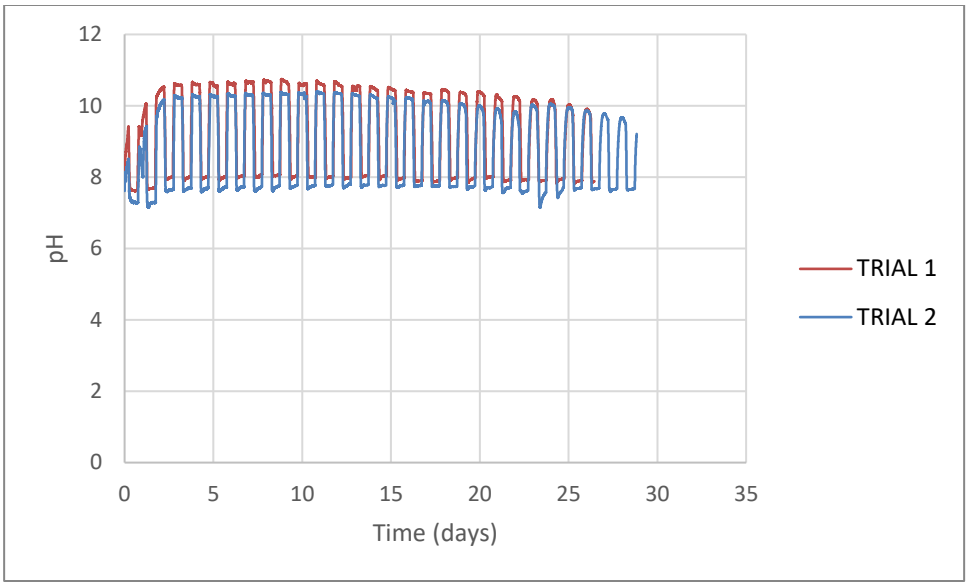

Figure 4.4: pH over time in air trials

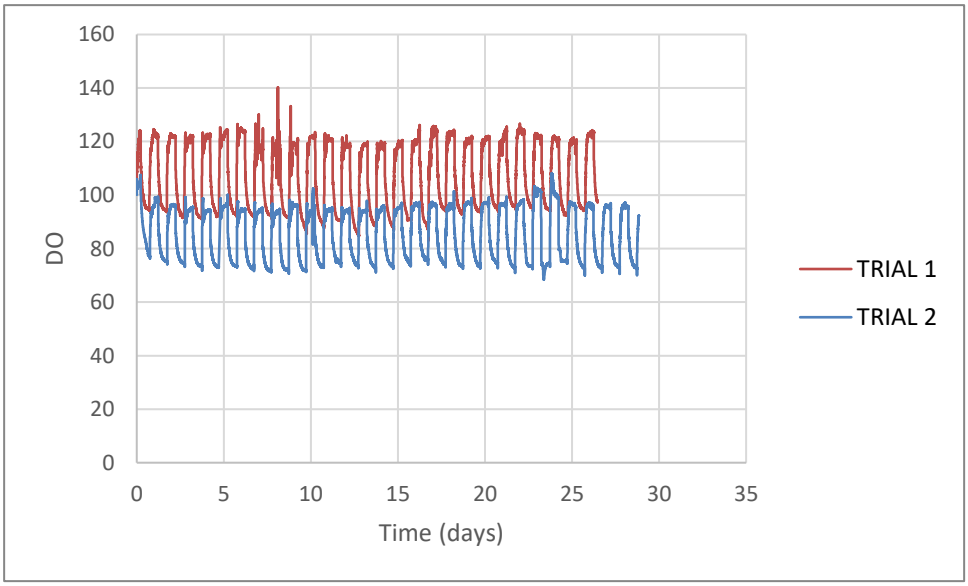

Figure 4.5: DO over time in air trials

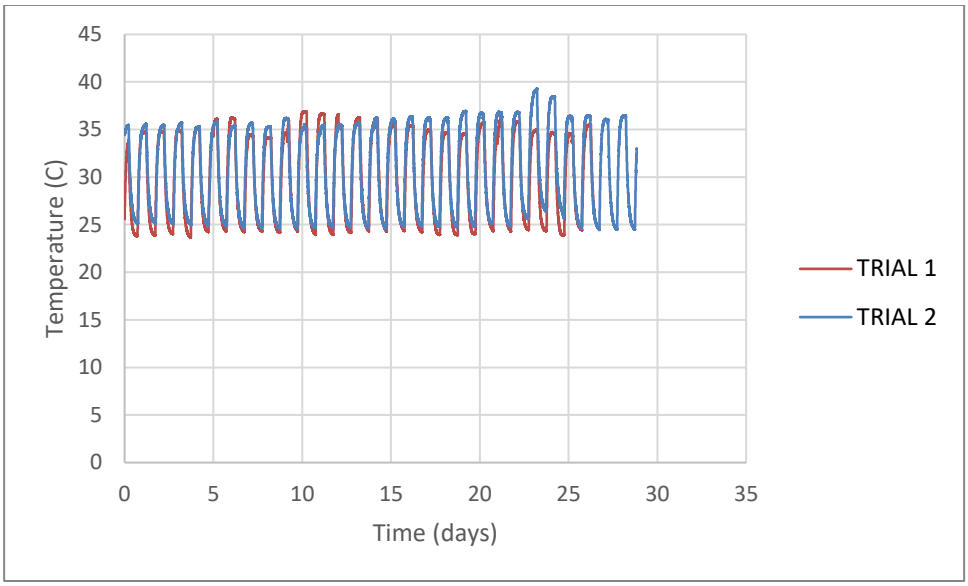

Figure 4.6: Temperature over time in air trials

In addition to the experiments using only air, algae growth experiments were run with varied CO_2 feed gas levels of 5%, 3.5%, 1.8%, 0.8%, 0.3%, and 0.15%. The results of these growth experiments along with the model fits are shown in Figures 4.7-4.12.

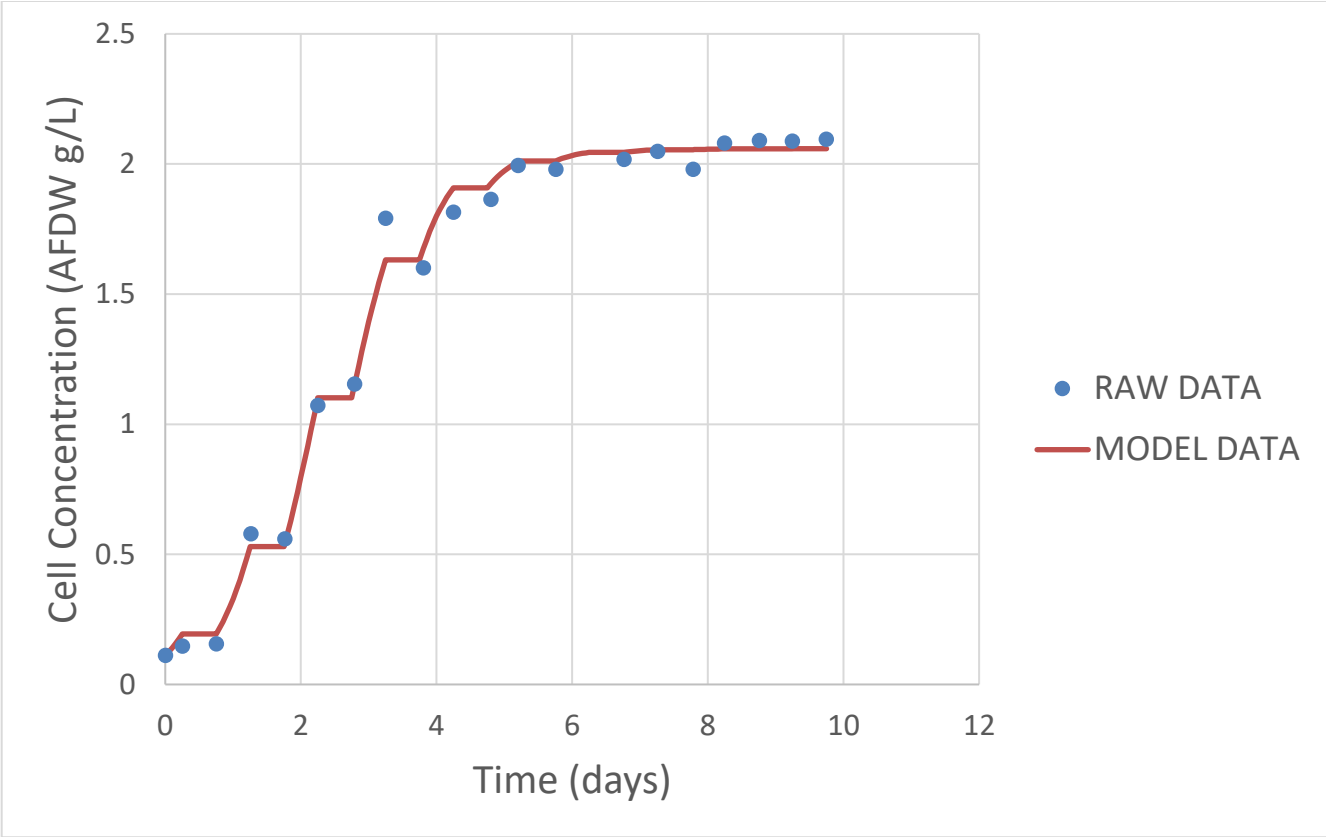

Figure 4.7: Chlorella sorokiniana growth in 5% CO_2 feed gas with a fit growth constant of 2.40 day^{-1} and an X_M of 2.06 g/L

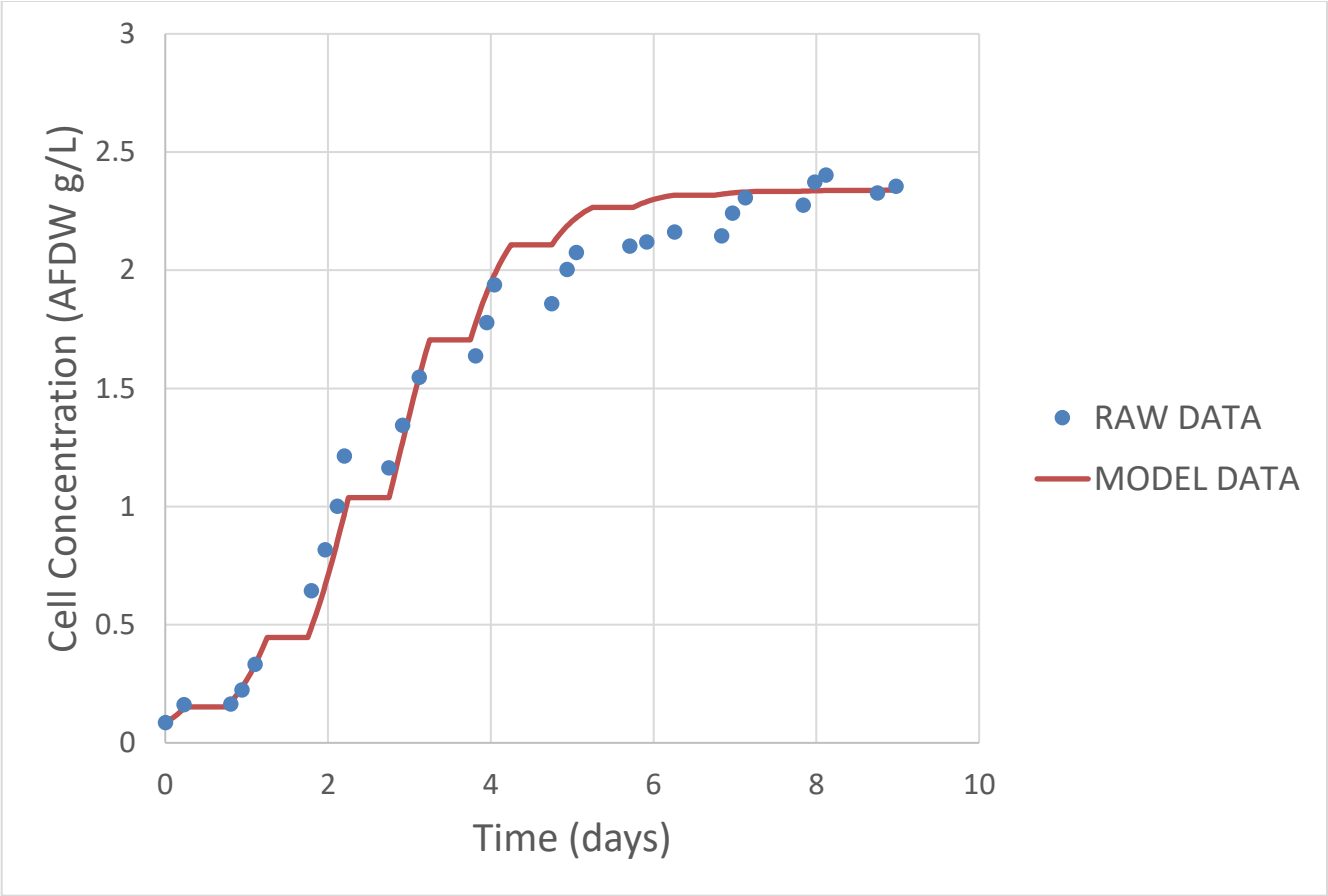

Figure 4.8: Chlorella sorokiniana growth in 3.5% CO_2 feed gas with a fit growth constant of 2.44 day^{-1} and an X_M of 2.34 g/L

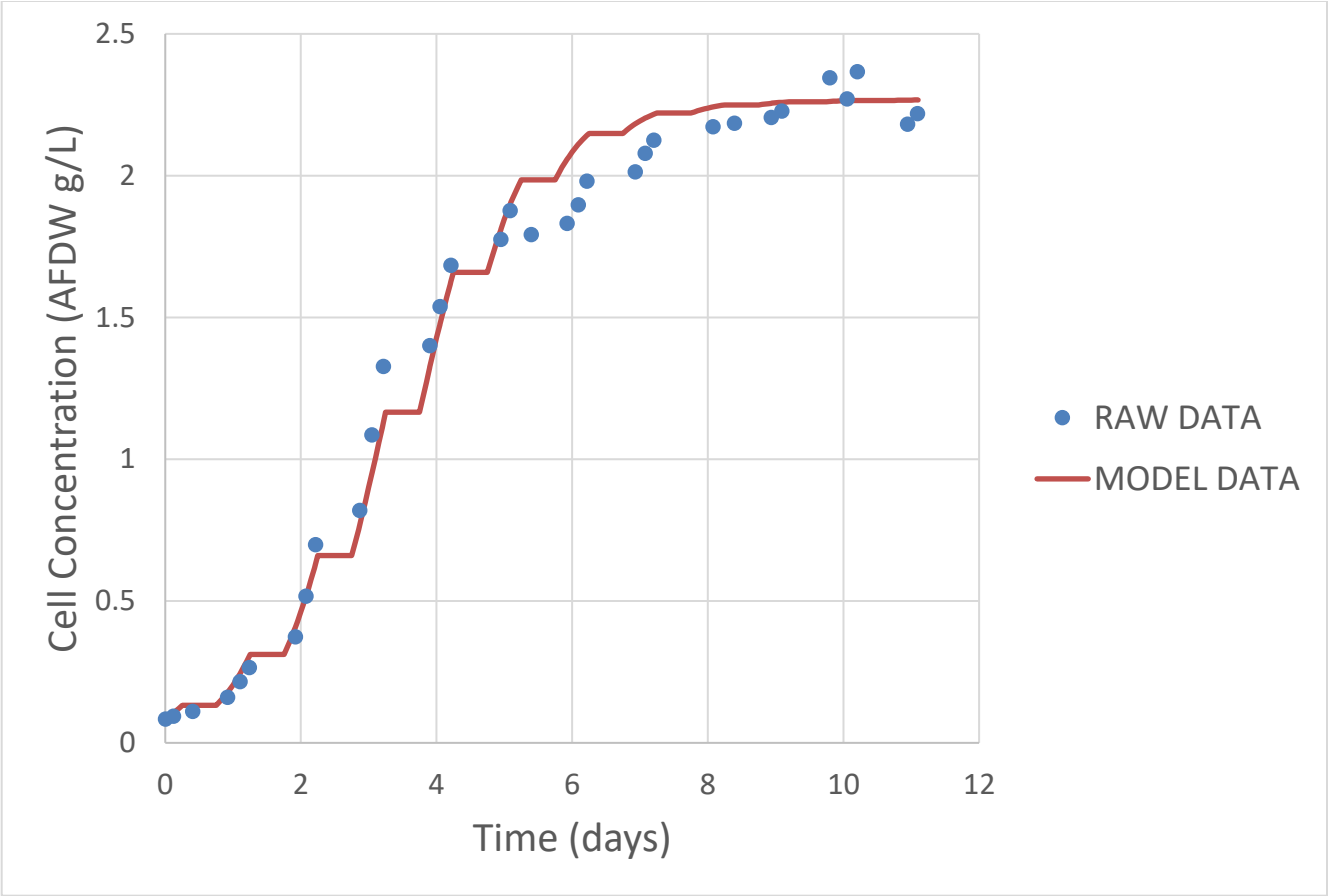

Figure 4.9: Chlorella sorokiniana growth in 1.8% CO_2 feed gas with a fit growth constant of 1.89 day^{-1} and an X_M of 2.27 g/L

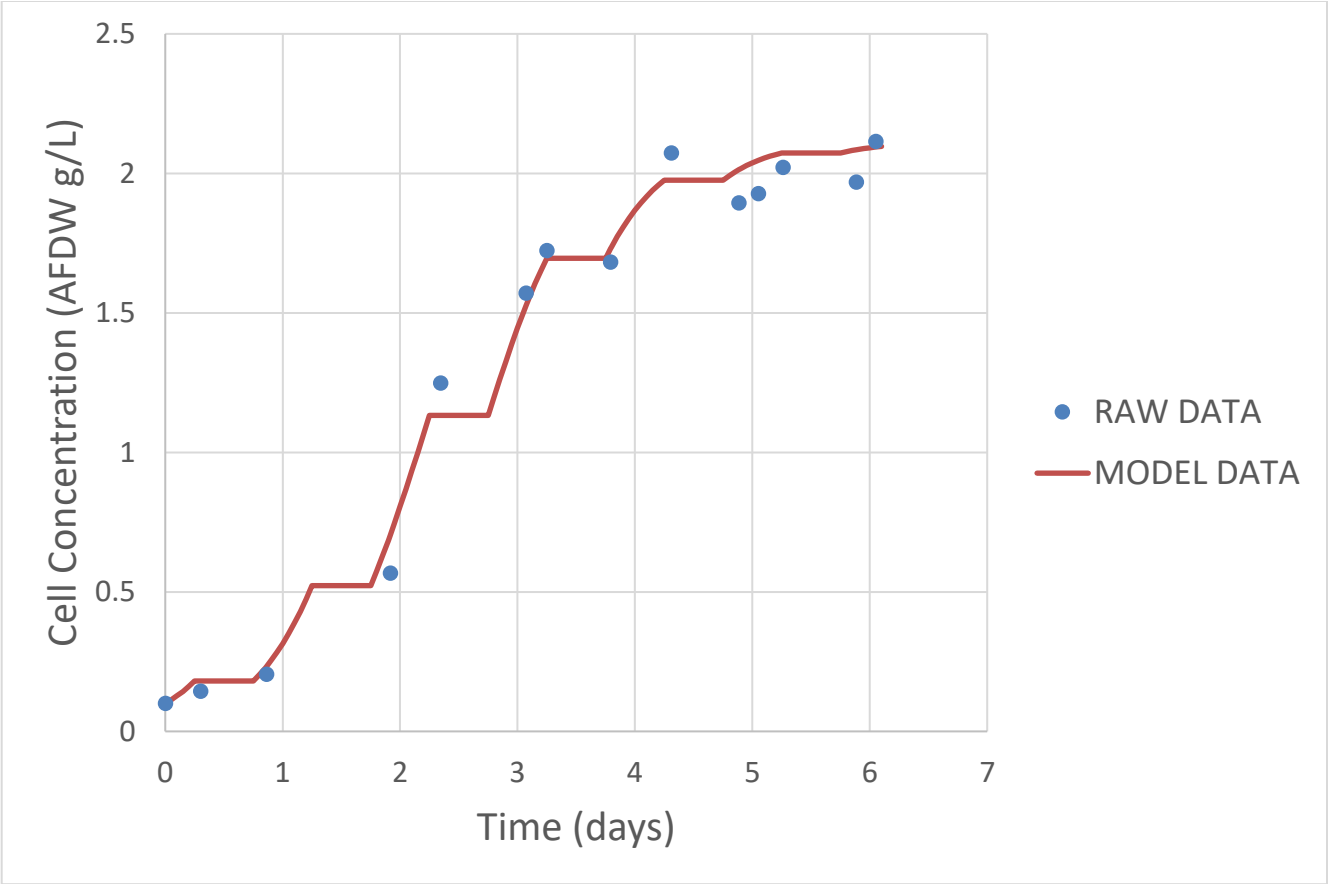

Figure 4.10: Chlorella sorokiniana growth in 0.8% CO_2 feed gas with a fit growth constant of 2.51 day^{-1} and an X_M of 2.11 g/L

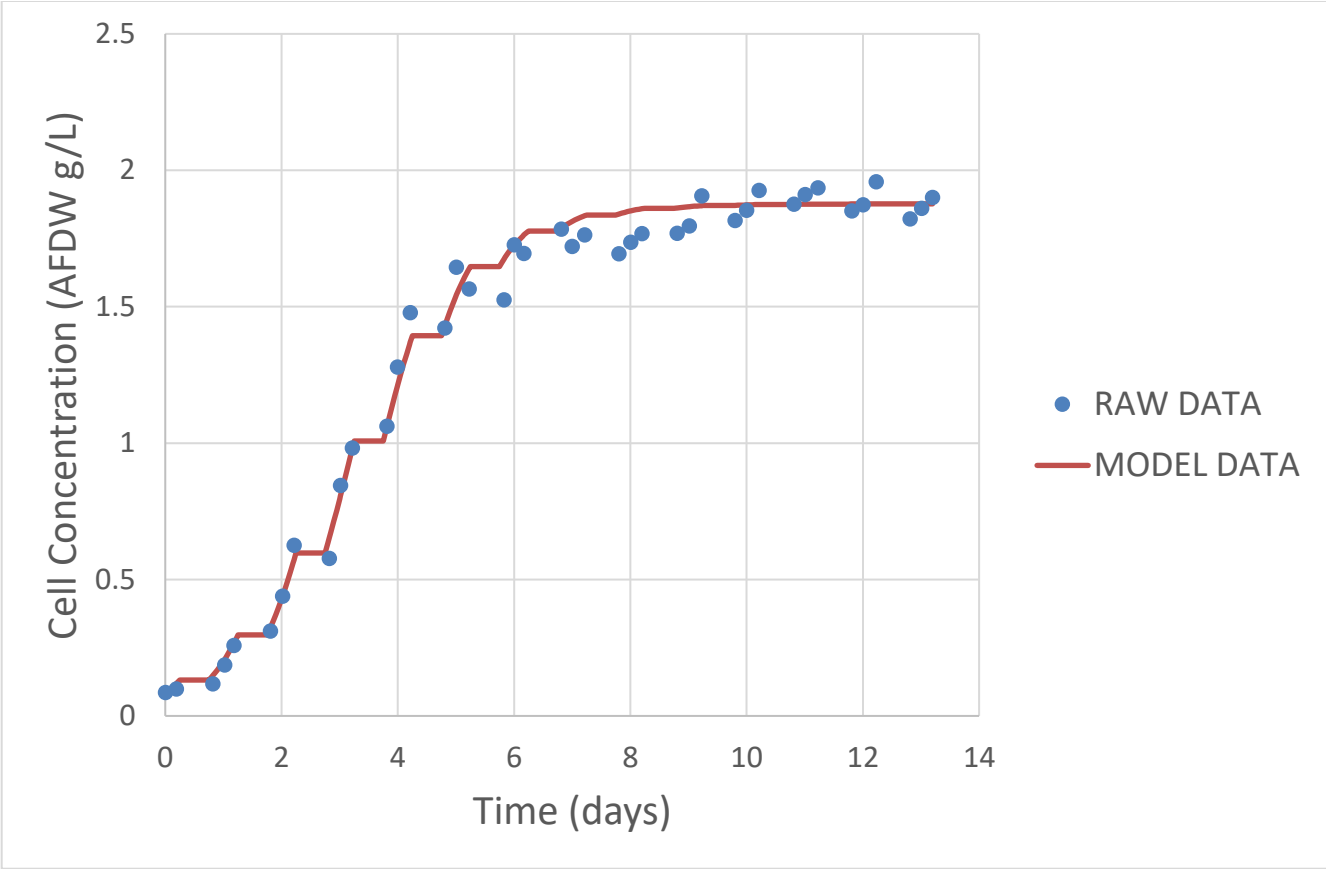

Figure 4.11: Chlorella sorokiniana growth in 0.3% CO_2 feed gas with a fit growth constant of 1.82 day^{-1} and an X_M of 1.88 g/L

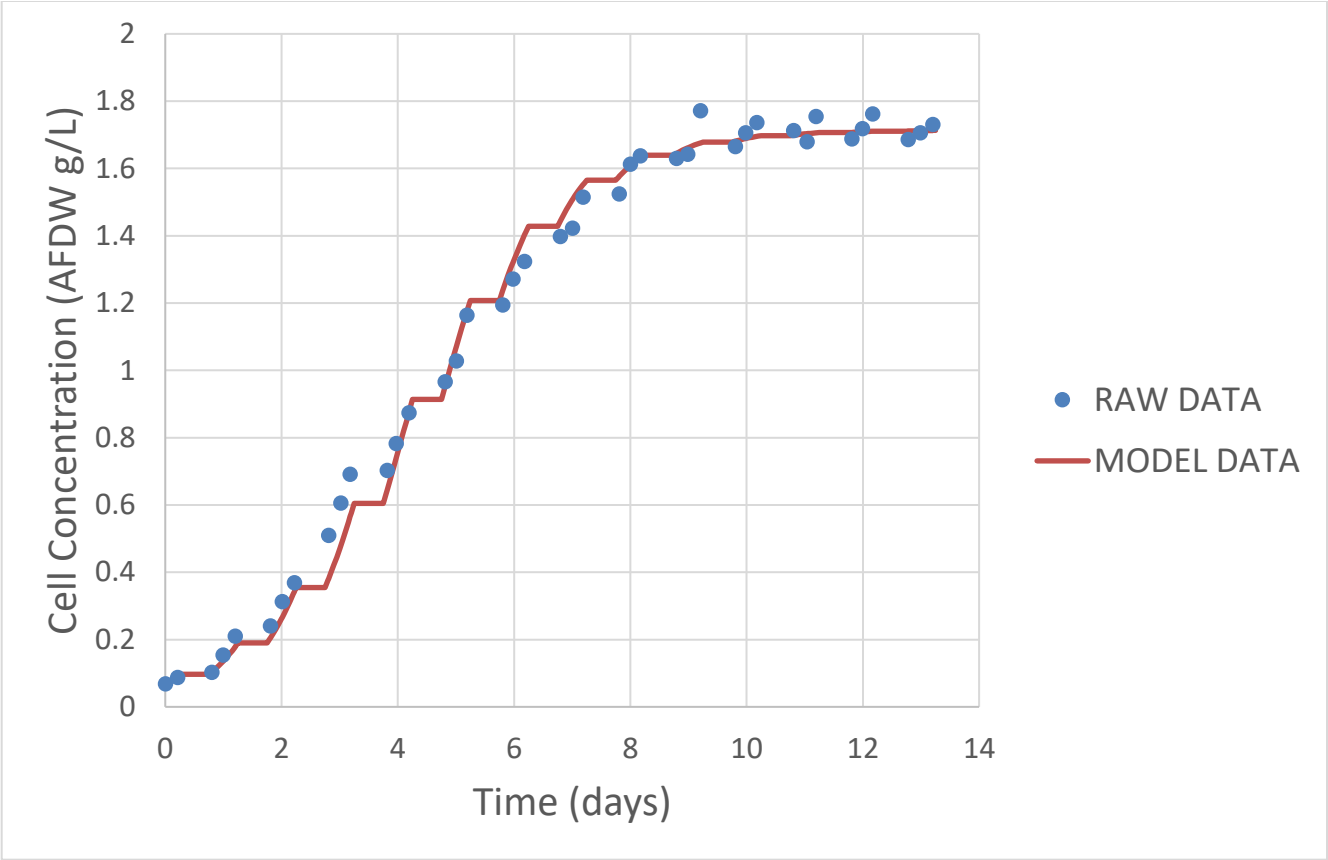

Figure 4.12: Chlorella sorokiniana growth in 0.15% CO_2 feed gas with a fit growth constant of 1.47 day^{-1} and an X_M of 1.72 g/L

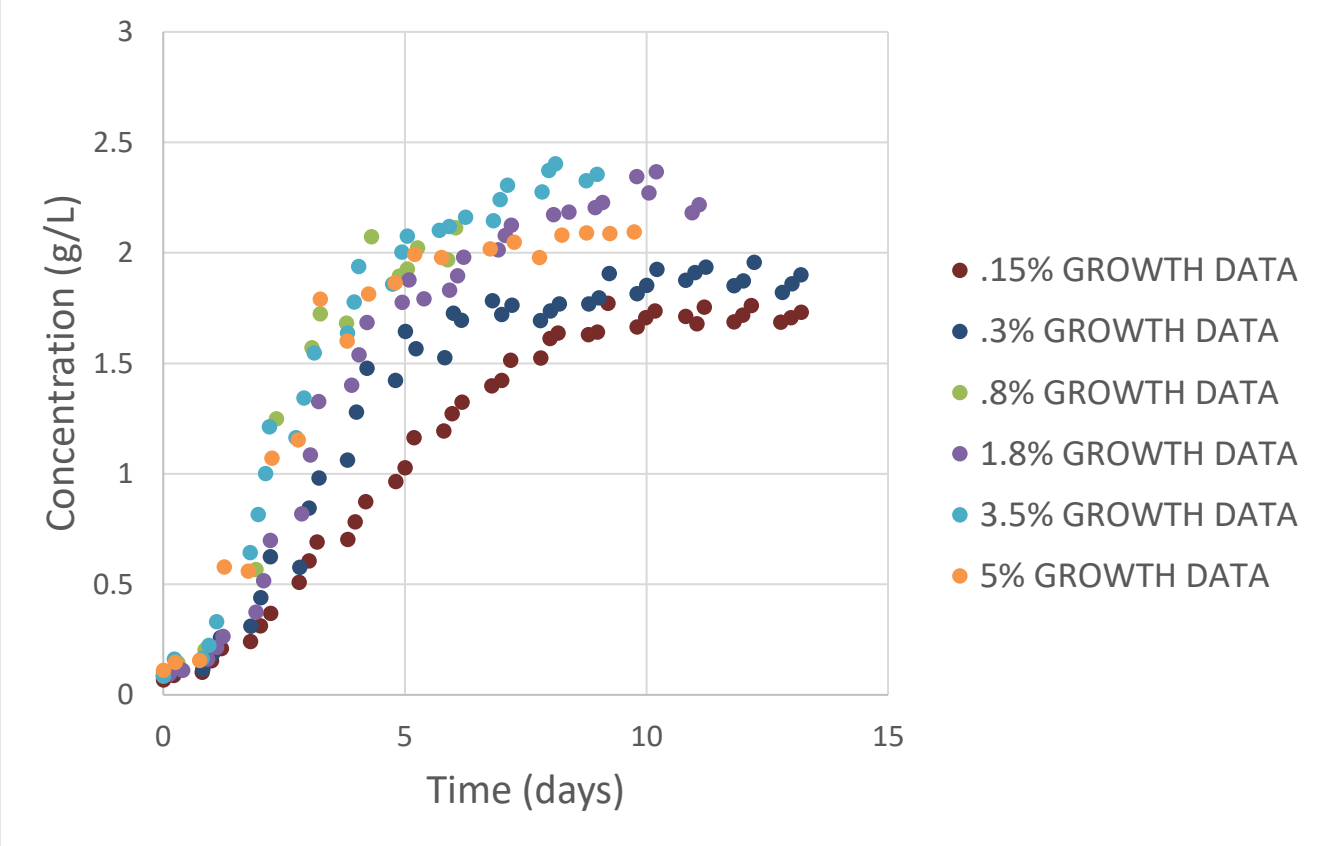

Figure 4.13: Chlorella sorokiniana growth in different CO_2 feed gas compositions

As seen in Figure 4.13, the growth between the 0.8%, 1.8%, 3.5%, and 5% CO_2 feed gas runs are comparable, with the 0.3% and 0.15% feed CO_2 noticeably resulting in both slower and less overall growth. From this, it can reasonably be considered that the 0.8% and up runs were fed more CO_2 than could be taken up by the algae. As a result, the 0.8% and up runs were combined into a single model shown in Figure 4.14.

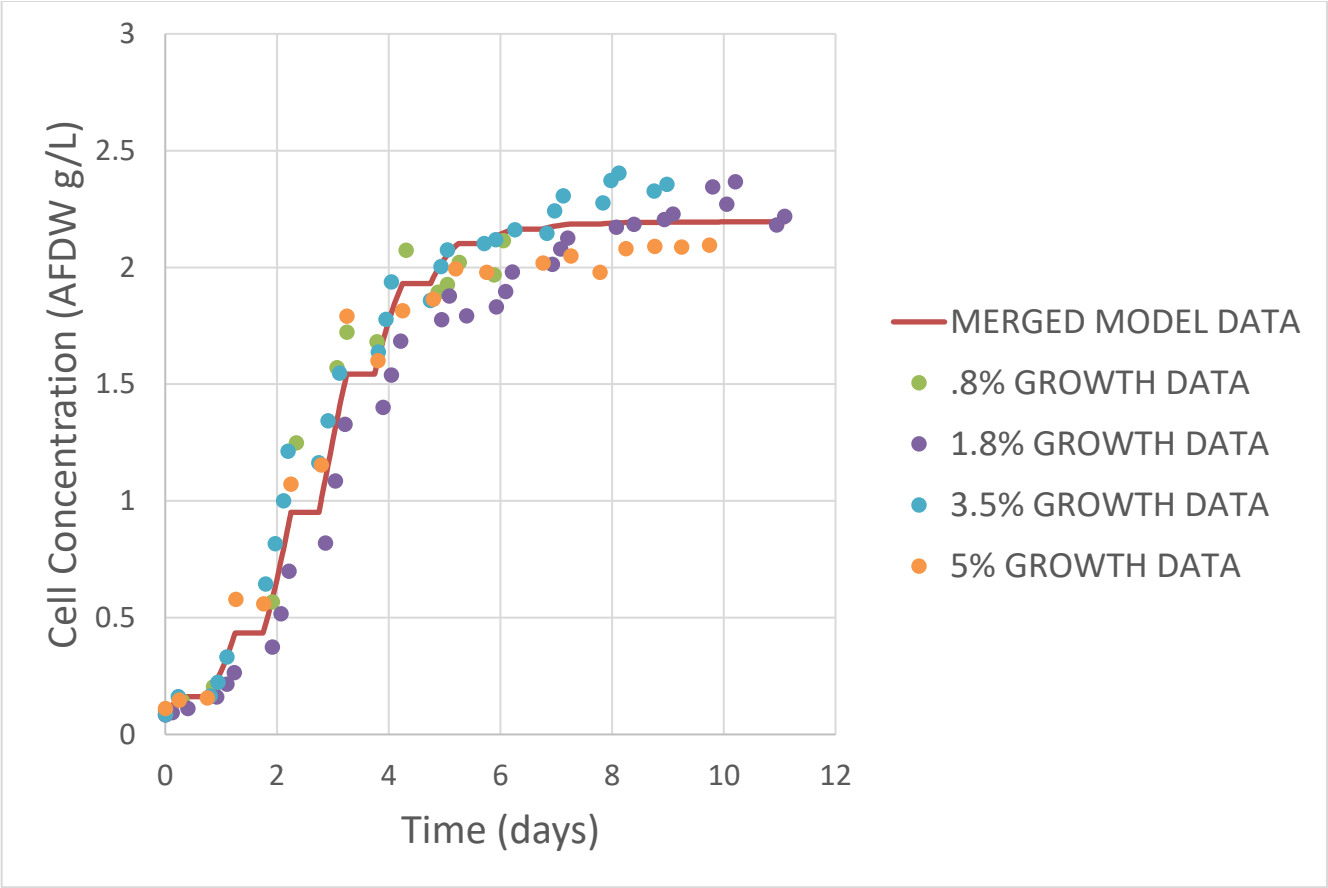

Figure 4.14: Chlorella sorokiniana growth in 0.8%-5% CO_2 feed gas with a merged fit growth constant of 2.26 day^{-1} and an X_M of 2.20 g/L

Although the four runs charted here result in similar maximum concentrations and growth constants, the growth constant for the 1.8% run is substantially lower than the others. It is unclear why this is but may be at least partially due to the inherent variability in biological growth [8].

In the 0.3% and 0.15% runs, the algae had a noticeably lower growth constant and maximum growth than the merged fit of the other four compositions, but still significantly higher than the air trials. This is shown more succinctly in Figure 4.15. This shows that the growth in these runs is limited by the availability of CO_2. The experimental data and fit growth constants for each run are shown in Table 4.1 along with the regression fit of the model. The growth constants found using this model are generally consistent with those found in previous studies [19].

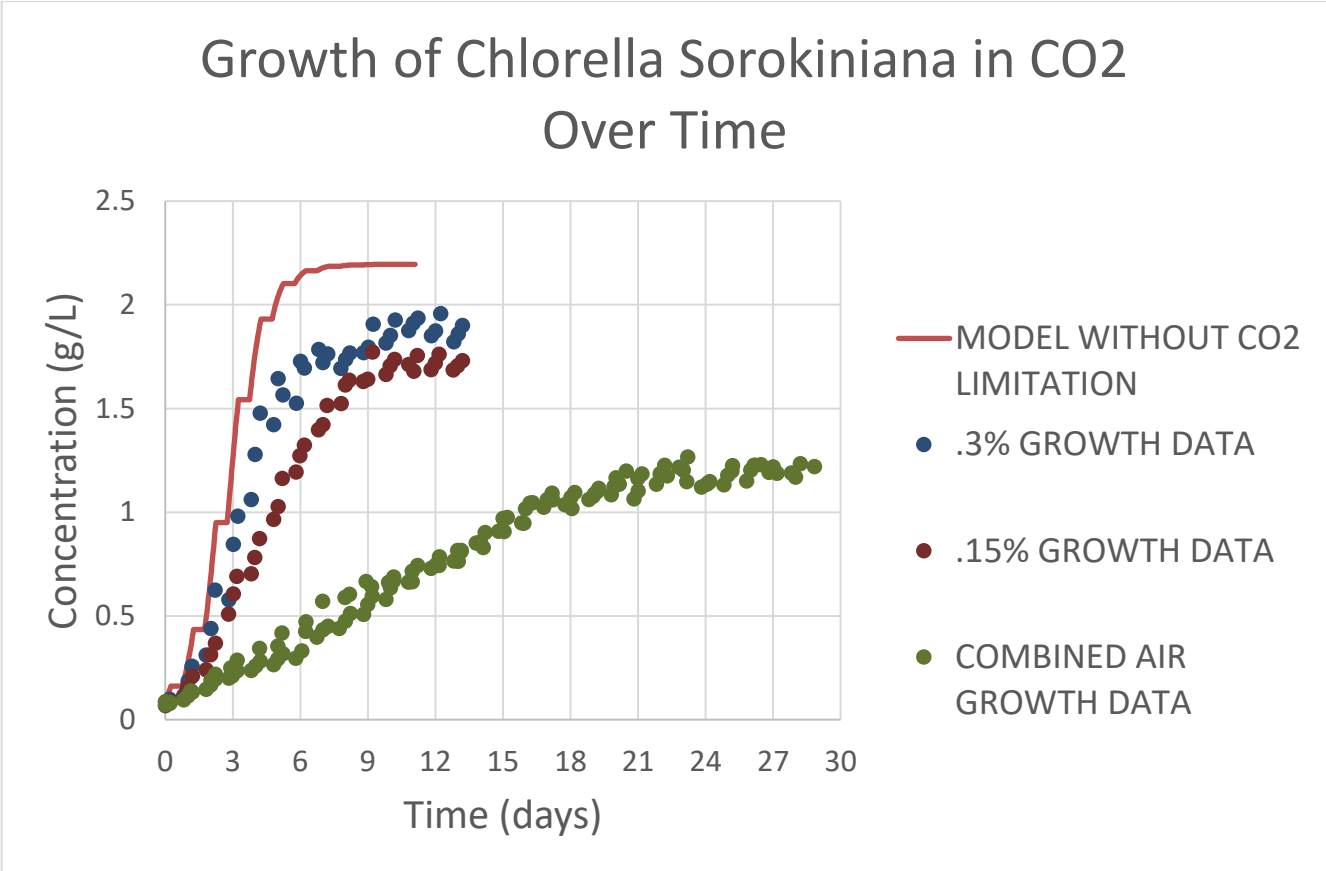

Figure 4.15: 0.8%-5% CO_2 feed gas merged fit shown alongside 0.3%, 0.15%, and air feed gas Chlorella sorokiniana growth

Table 4.1 – Growth Modeling Data

Run	**X_0 (g/L)**	**X_M (g/L)**	**μ (growth constant) (1/day)**	**r^2**
5%	0.111	2.06	2.40	0.994
3.5%	0.0855	2.34	2.44	0.975
1.8%	0.0843	2.27	1.89	0.984
0.8%	0.100	2.11	2.51	0.988
Merged 0.8%+	0.0954	2.20	2.26	0.964
0.3%	0.0857	1.88	1.82	0.990
0.15%	0.0680	1.72	1.47	0.993
Air Combined	0.0789	1.19	0.550	0.981

For each trial, the pH, DO, and temperature were recorded over time. It is worth noting that computer errors led to only capturing part of this data for the 3.5% and 5% runs. The trends in temperature were relatively similar in each run, including in air. This is to be expected as the light source was the main source of heat in the experiments. The light intensity was held constant throughout each trial. These trends are seen in Figure 4.16 for non-air runs. The lower peaks seen in the 0.15% CO_2 can likely be attributed to the distance between the light source and the reactor. The troughs occur during the dark phase of the growth and reflect the temperature of the room in which the experiments were conducted.

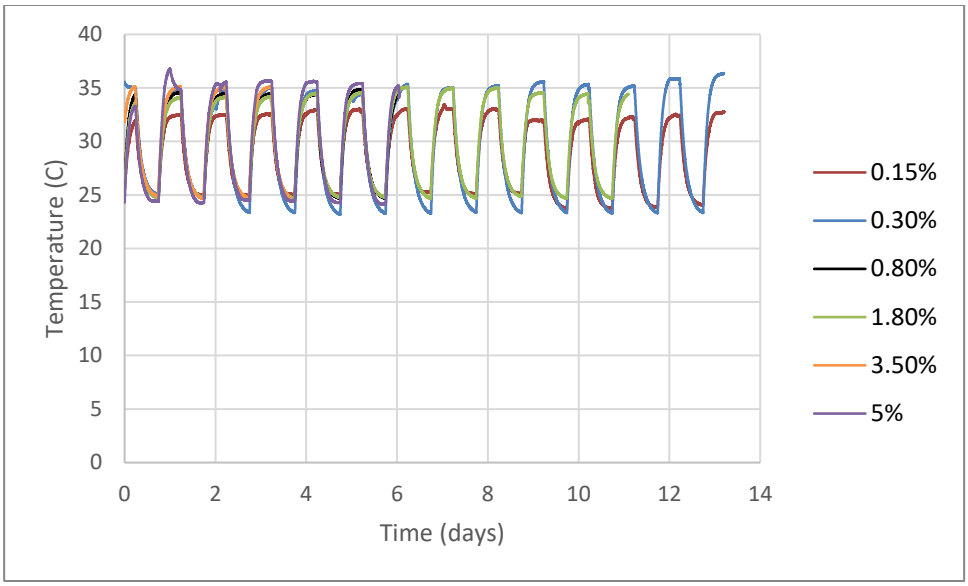

Figure 4.16: Temperature over time in all runs excluding air

Additionally, the DO trends were similar between runs. As shown in Figure 4.17, DO peaks increase by day in the beginning of the runs but the trend is reversed after 2-3 days. This corresponds with the apparent growth rates of the algae. The highest apparent rates of growth happen within the first few days in all runs around day 2-3 and then the apparent rate of growth decreases throughout, consistent with the DO trends. This is shown in the observed rate of change in the cell concentration.

The 0.15% and 0.3% runs have noticeably lower peaks than the other runs. This lines up with the substantially lower growth in these runs. This supports that higher DO levels correspond to more growth and that the lower levels of CO_2 that limit growth led to lower DO levels. Similarly to the temperature, the DO levels dropped significantly during the dark phase of the cycle. This is to be expected due to the decreased algae respiration when deprived of light [38].

Overall, the variability in the DO level of the runs with CO_2 was higher than that of pure air, with the 0.15% behaving similarly to air. This suggests that when the DO chart over time has no significant trend in the peaks, the growth is significantly CO_2 limited.

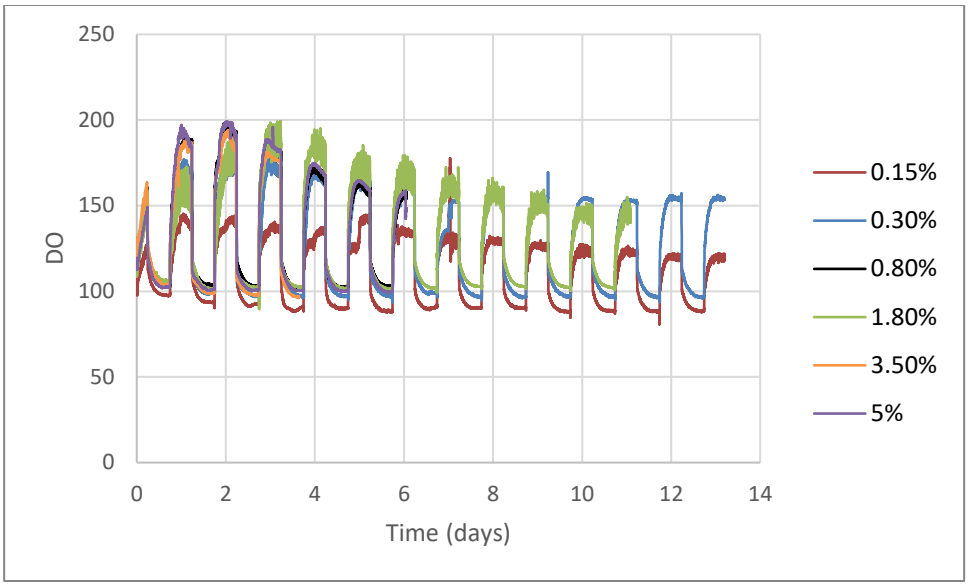

Figure 4.17: Dissolved oxygen (DO) over time in all runs excluding air

The other variable monitored was the pH over the duration of each run. The pH between the CO_2 runs varied significantly with CO_2 level. This is shown in Figure 4.18. The pH for the 0.3% and the 0.15% runs were significantly higher than the pH in the 0.8%, 1.8%, 3.5%, and 5% runs. As a result, the 0.8%, 1.8%, 3.5%, and 5% runs are shown separately on Figure 4.19. It can be seen that in all of the runs there is an initial drop in the pH. This is likely due to the initial shock of CO_2 to the system and the pH is dictated by this CO_2 rather than the algae growth. During the light phase of the experiments the pH increases as the algae is growing. During the dark phase of the cycle, the pH reaches a trough. This is due to the CO_2 controlling the pH while the algae have no light to grow.

The pH on the air runs had the most variability. This is because there was no additional CO_2 to lower and buffer the pH. Therefore, the fluctuations in pH were caused mainly by the growth cycle of algae.

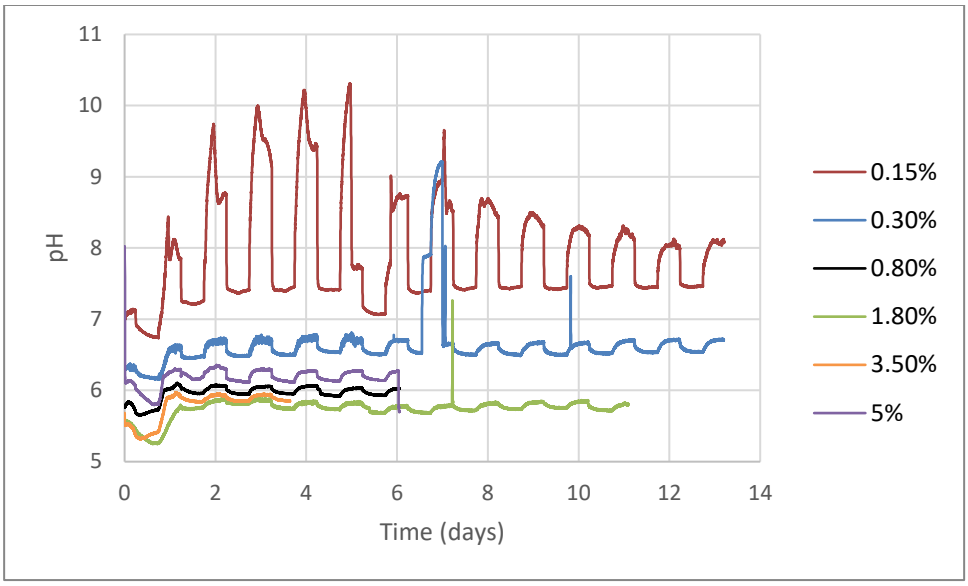

Figure 4.18: pH over time in all runs excluding air

It can be seen in the graphs of the 0.15% and the 0.3% runs that there are periods in which the pH seems to peak much higher than would be expected. This is likely due to the CO_2 levels dropping. This is consistent with errors in the experimentation. During the first few days of the 0.15% run, the regulator on the CO_2 was not set up correctly, leading to a lower pressure of CO_2 delivered than intended. During the 0.3% run the CO_2 became disconnected for a few hours during the day, also resulting in less CO_2 delivery. Similarly, during the 1.8% run the CO_2 became disconnected for a few minutes while the water in the flask was replaced, leading to the recorded spike in pH.

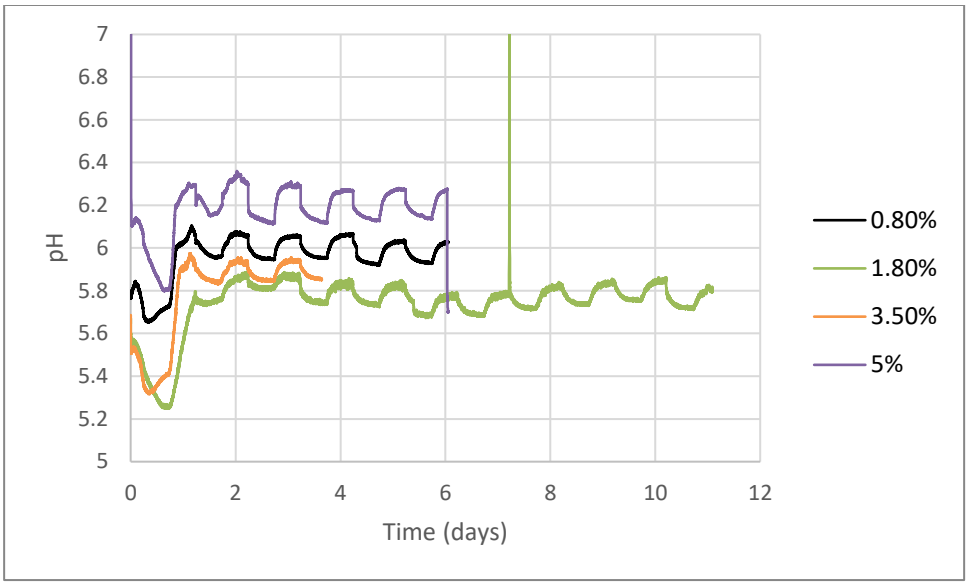

Figure 4.19: pH over time in all runs excluding air, 0.15%, and 0.3%

As seen in Figure 4.19, there is no real trend in pH regarding CO_2 percentage. All these runs resulted in similar pH data. This can be reasonably explained by the presence of excess CO_2 in all runs, which is consistent with the growth trends.

4.2 Dynamic pH Results and Discussion

To further understand the CO_2 dissolution in media and the effects on the growth, the pH was modeled over time using the convective mass transfer between the gas bubbles and the media. In the dynamic pH modeling experiments, PECOS media and other solutions were used to test the convective mass transfer model developed in Equation 26. There were many constants obtained from literature [9] and are recorded in Table 4.2.

Table 4.2 – Helpful Constants in Dynamic pH Model – Constants at 25º C

Constant Name	**Constant Symbol**	**Value**	**Units**
Henry's Constant	K_H	$10^{-1.47}$	mol/Latm
Equilibrium Constant 1 (Equation 3)	K_{a1}	$10^{-6.35}$	unitless
Equilibrium Constant 2 (Equation 4)	K_{a2}	$10^{-10.33}$	unitless
Water Ionization Constant	K_W	10^{-14}	mol^2/L^2

In addition to these constants, the sodium ion concentration in each media was also important to get an accurate relationship between pH and time. This sodium ion concentration, denoted as [+], significantly changes the m and b values from Equation 17 used in the model. An example of the difference is shown in Figure 4.20. These values are shown in Table 4.3.

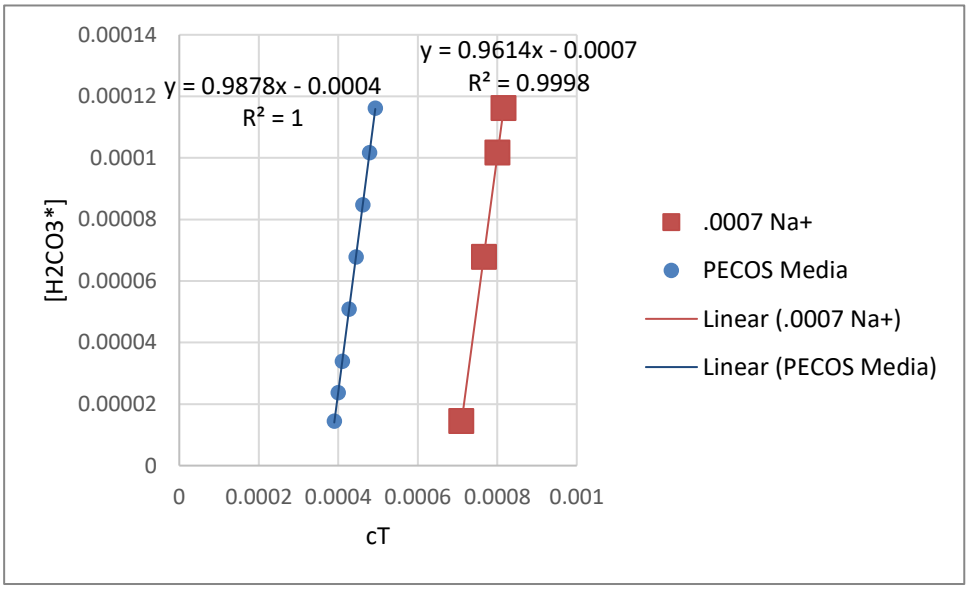

Figure 4.20: Comparison of sodium ion concentration effect on relation between c_T and $[H_2CO_3^*]$

Table 4.3 – Sodium Ion Concentrations Across Medias

Media	**[+] (mol/L)**	**m in model**	**b in model**
PECOS Media	3.77×10^{-4}	0.9878	-3.711×10^{-4}
DI Water	0	0.9864	-5.469×10^{-6}
Basic Solution 1	8.47×10^{-4}	0.9992	-8.458×10^{-4}
Basic Solution 2	6.99×10^{-4}	0.9974	-6.946×10^{-4}

When modeling the dynamic pH, it was important to know the P_{CO_2}. In the experiments, house air was used, as well as the BioFlo system. The P_{CO_2} in these trials was not certain and could be determined through the equilibrium states of these trials using Equation 14. However, initially values were used for P_{CO_2} that corresponded to nominal values of CO_2 percentage in air of 427 parts per million [39].

The first experiments using PECOS media were meant to find the convective mass transfer coefficients using the BioFlo system with 0.3% CO_2 and air; with a P_{CO_2} of 0.003427 and 0.000427 respectively. These mass transfer coefficients could be found using Equation 26 and solver to maximize the r^2 in Equation 3, an optimal $k_c a$ could be found. It was hypothesized that the coefficient values would be the same in the absorption and desorption of the 0.3% CO_2 due to the use of the same media. The media was saturated with air before adding 0.3% CO_2 to re-saturate the media. Afterwards, the media was again saturated with air by continuing gas flow without CO_2. The data and model equations are shown in Figures 4.21 and 4.22 using the optimal convective mass transfer coefficient found from the fit of the 0.3% P_{CO_2} in the PECOS media.

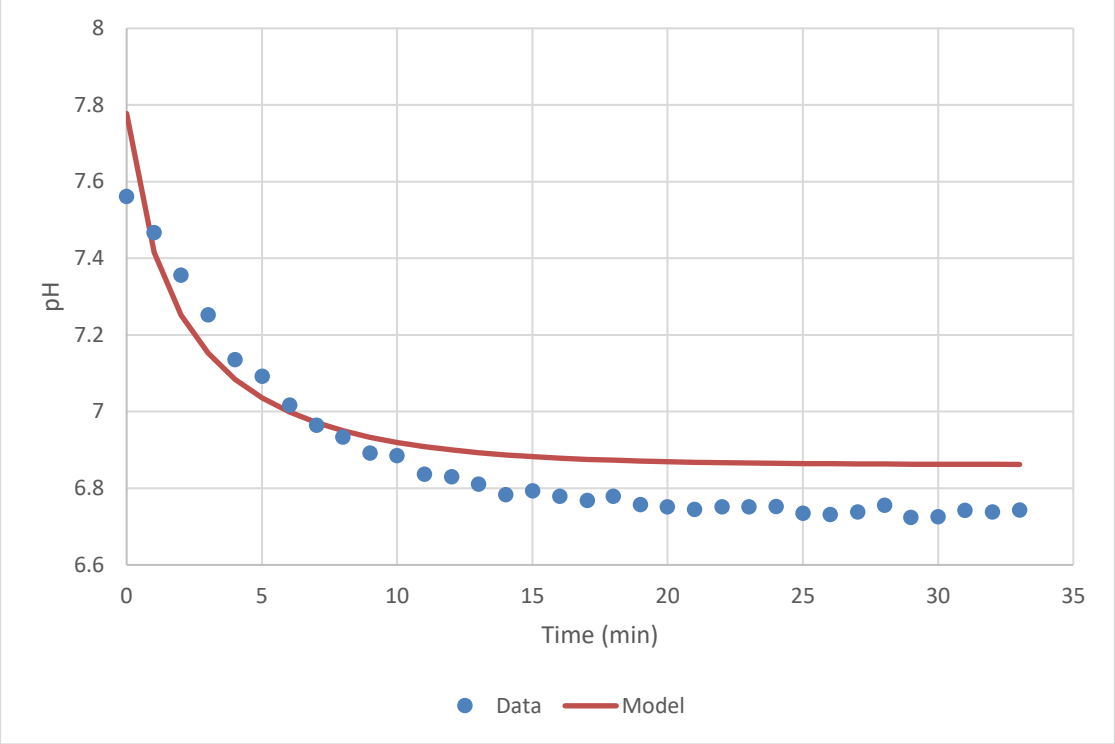

Figure 4.21: pH over time of 0.3% CO_2 in PECOS media, P_{CO_2}=0.003427 atm, k_ca=0.197 min^{-1}

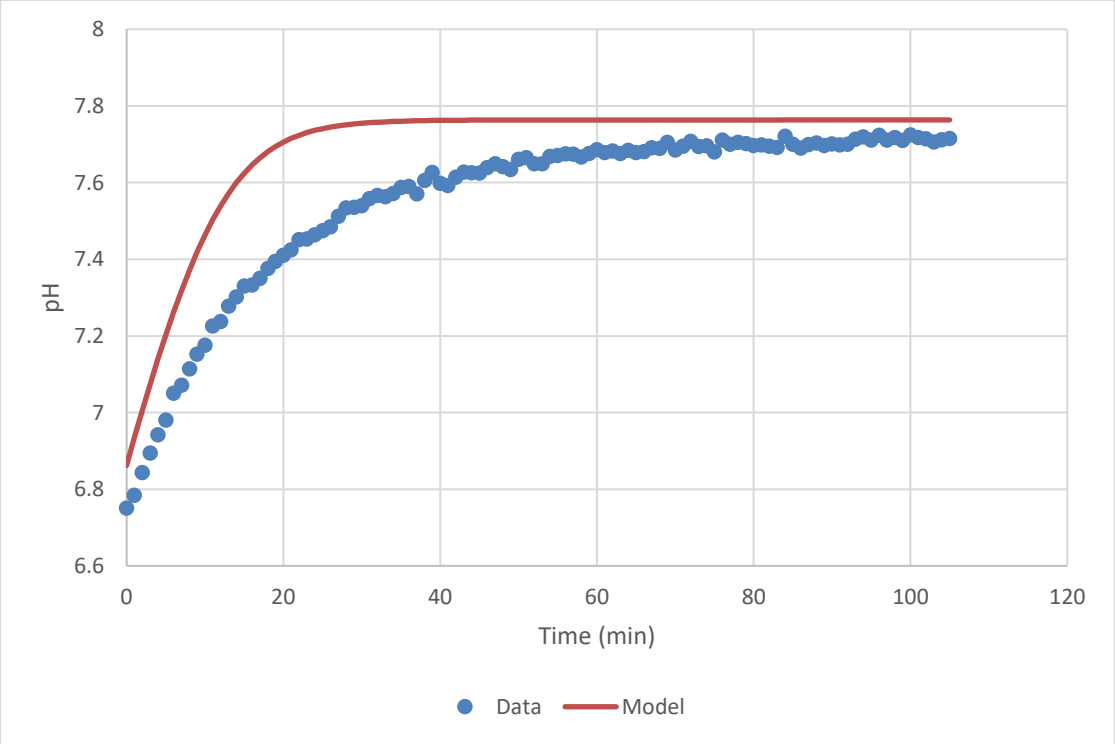

Figure 4.22: pH over time of air in PECOS media, P_{CO_2}=0.000427 atm, k_ca=0.197 min^{-1}

Neither of these two fits was particularly accurate, but a good fit was obtained for air re-saturation when the $k_c a$ was found with solver. This re-fit of the convective mass transfer coefficient can be seen in Figure 4.23. This shows that this model can be accurately used to represent the dynamic pH trends of the dissolution of CO_2 in aqueous media.

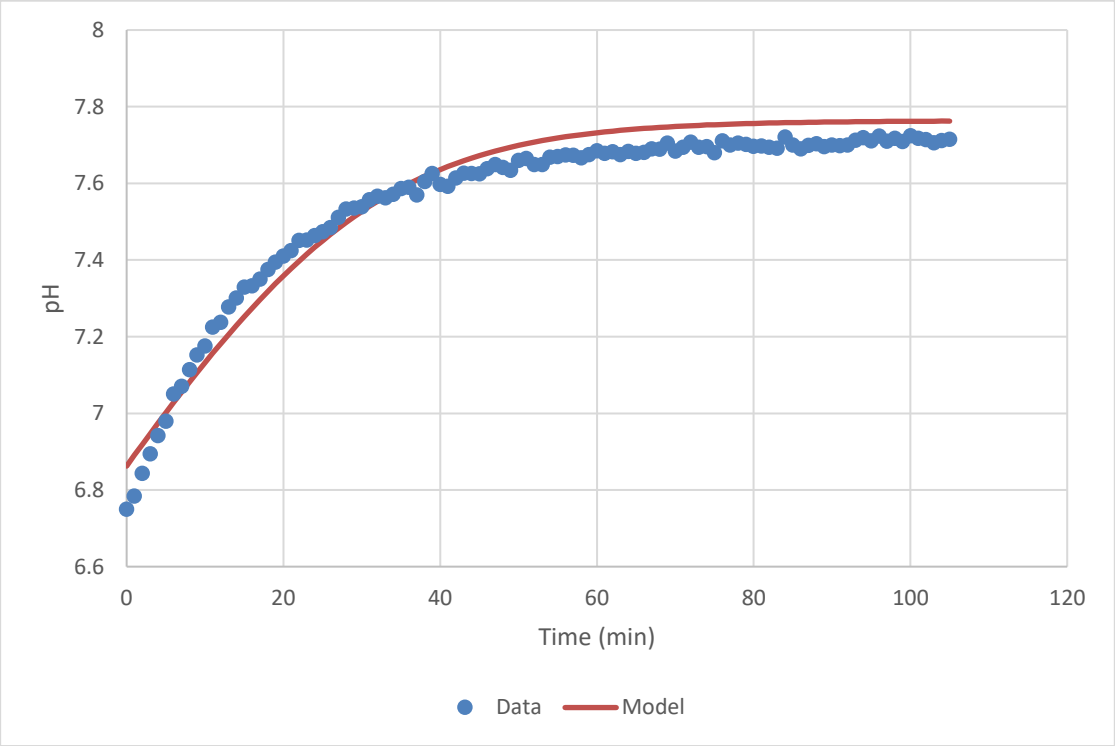

Figure 4.23: Refit of pH over time of air in PECOS media, P_{CO_2}=0.000427 atm, $k_c a$=0.0765 min^{-1}

However, these models did not accurately reflect the initial and final pH of the data. As a result, it was hypothesized that the P_{CO_2} values used were not accurate. When finding new P_{CO_2} values for the experiments, Equation 14 was used along with the pH relation to $[H^+]$ to be able to solve for new P_{CO_2} values from the equilibrium pH values of 6.74 and 7.71 respectively. New P_{CO_2} values were found for both air and 0.3% CO_2 of 0.00452 and 0.000486 respectively. Using these P_{CO_2} values, a new convective mass transfer coefficient was found for CO_2 adsorption. The new fits using this coefficient for these data sets are shown in Figures 4.24 and 4.25. These new fits can be described with the same value of the convective mass transfer coefficient. The values used for the fits in the PECOS media are shown in Table 4.4.

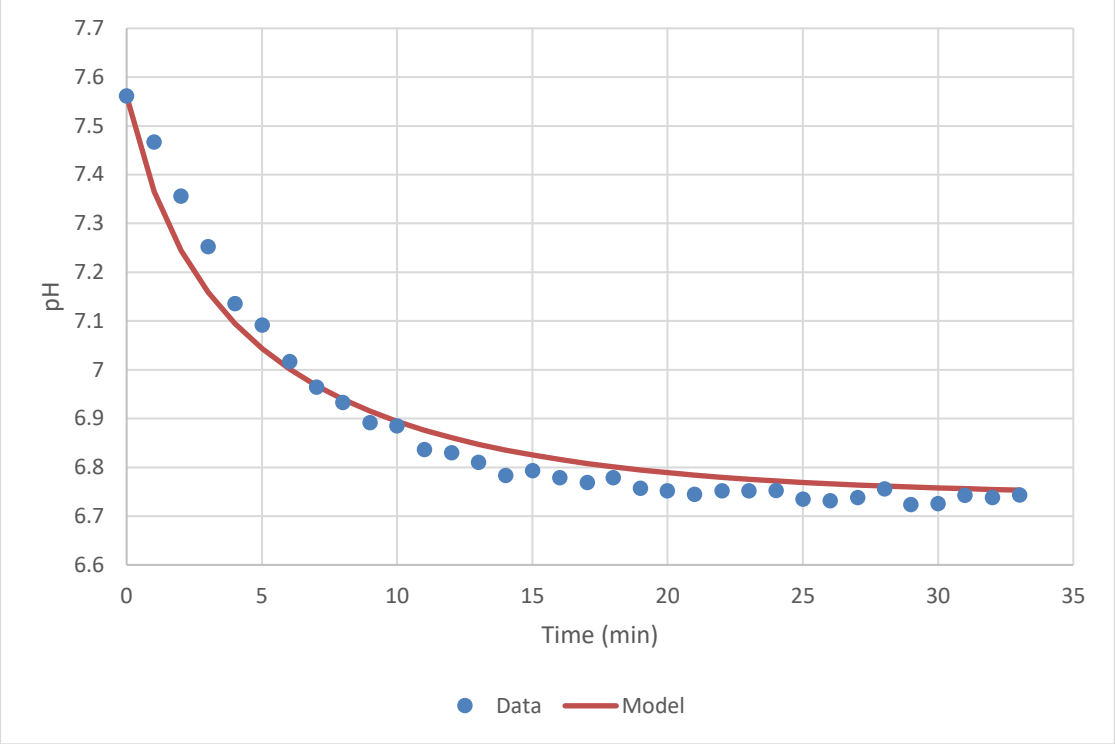

Figure 4.24: pH over time of 0.3% CO_2 in PECOS media, P_{CO_2}=0.00452 atm, $k_c a$=0.106 min^{-1}

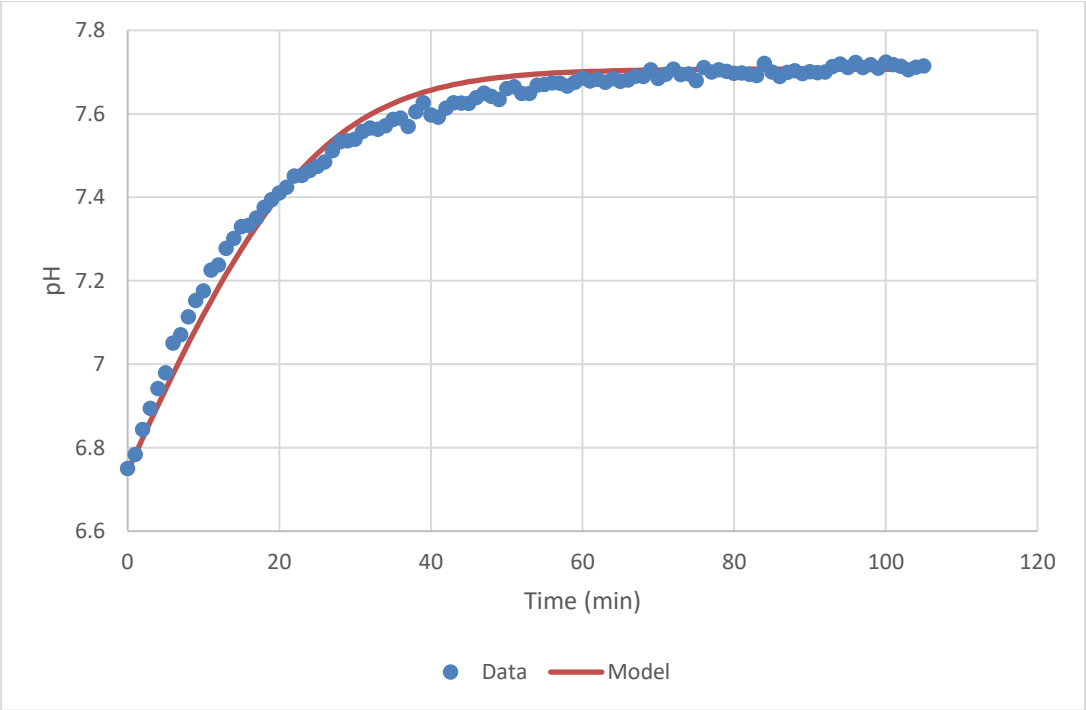

Figure 4.25: pH over time of air in PECOS media, P_{CO_2}=0.000486 atm, $k_c a$=0.106 min^{-1}

Table 4.4 – Results for PECOS Media Dynamic pH Experiments

Run	**c_{T0} (mol/L)**	**P_{CO_2} (atm)**	**$k_c a$ (min^{-1})**	**r^2**
0.3% Original	3.899 x 10^{-4}	0.003427	0.197	0.777
Air Original	4.931 x 10^{-4}	0.000427	0.197	0.501
Re-Fit Air	4.931 x 10^{-4}	0.000427	0.0765	0.951
0.3% New P_{CO_2}	3.991 x 10^{-4}	0.00452	0.106	0.964
Air New P_{CO_2}	5.302 x 10^{-4}	0.000486	0.106	0.981

From this data it can be concluded that the new fits for the P_{CO_2} values are more accurate. This is because the new values of $k_c a$ allow for a better fit of the experimental data with the model. Additionally, the optimized $k_c a$ value is the same for both saturation and desaturation of CO_2 in air.

In addition to the experiments run in the PECOS media, experiments were conducted with three different flowrates in DI water to confirm the P_{CO_2} values obtained in the new PECOS trials were accurate. There was not enough data collected in these trials in DI water to model the dynamic pH.

Equilibrium data was used to find the P_{CO_2} of the gas in DI water. Data is shown for these confirmation runs in Table 4.5. In addition to the confirmation of the P_{CO_2} in PECOS, there was an experiment performed in DI water using 5% CO_2 unmixed with additional air for future reference during runs using base solutions.

Table 4.5 – Results for Experiments in DI Water

Run	**Equilibrium pH**	**P_{CO_2} (atm)**	**P_{CO_2} (atm) from PECOS**	**% Difference**
0.3% in DI	5.06	0.00490	0.00452	8.07%
Air in DI	5.57	0.000480	0.000486	1.24%
5% in DI	4.55	.0536	N/A	N/A

These results show that these P_{CO_2} values for our experiments in Tucson, Arizona are likely accurate now that they have been confirmed in two different solutions. The higher P_{CO_2} value found in pure air can likely be attributed to the location of the experiments. Experiments were run on the University of Arizona campus which has air with higher than the global average composition of CO_2 due to the activity in the vicinity [40].

These results lend credibility to the accuracy of the 5% CO_2 P_{CO_2} calculated from the DI water trials. This means that the calculated 5% P_{CO_2} and the average of the two P_{CO_2} values for air runs found in Table 4.5 can be used in the model for the basic solutions. Additionally, the two charge values calculated at equilibrium for the base solutions were averaged to find the *m* and *b* values for the model, shown in Table 4.3. The calculated charges are shown in Table 4.6.

Table 4.6 – Calculated Charges in Basic Solutions (mol/L)

Run	**Air Saturation [+]**	**5% Saturation [+]**	**Average [+]**	**% Difference**
Basic Solution 1	8.25×10^{-4}	8.68×10^{-4}	8.47×10^{-4}	5.07%
Basic Solution 2	7.52×10^{-4}	6.46×10^{-4}	6.99×10^{-4}	15.2%

The data and fit models for Basic Solution 1 are shown in Figures 4.26 and 4.27. For this run, the optimal $k_c a$ values did not align for air and 5%. Similarly to the runs in the PECOS media, the constant was re-fit for the desorption of the CO_2 in Figure 4.28. This shows that there was some difference between the absorption and desorption of the CO_2 within the system. The value for $k_c a$ obtained for the desorption process fits the data more closely. It is hypothesized that the difference in the two $k_c a$ values of CO_2 absorption and desorption are due to possible discrepancies in the bubble size between the air and CO_2 feeds. This may be due to differences in feed line pressures, or that the BioFlo pushes the gases out at slightly different rates.

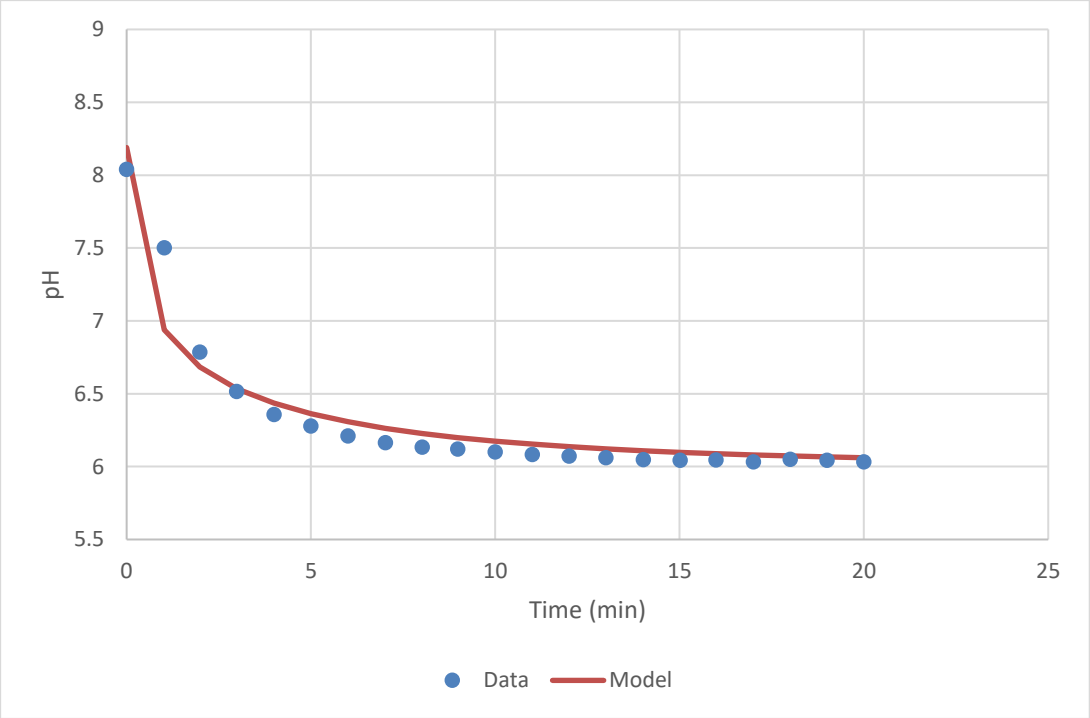

Figure 4.26: pH over time of 5% CO_2 in Basic Solution 1, P_{CO_2}=0.0536 atm, $k_c a$=0.119 min^{-1}

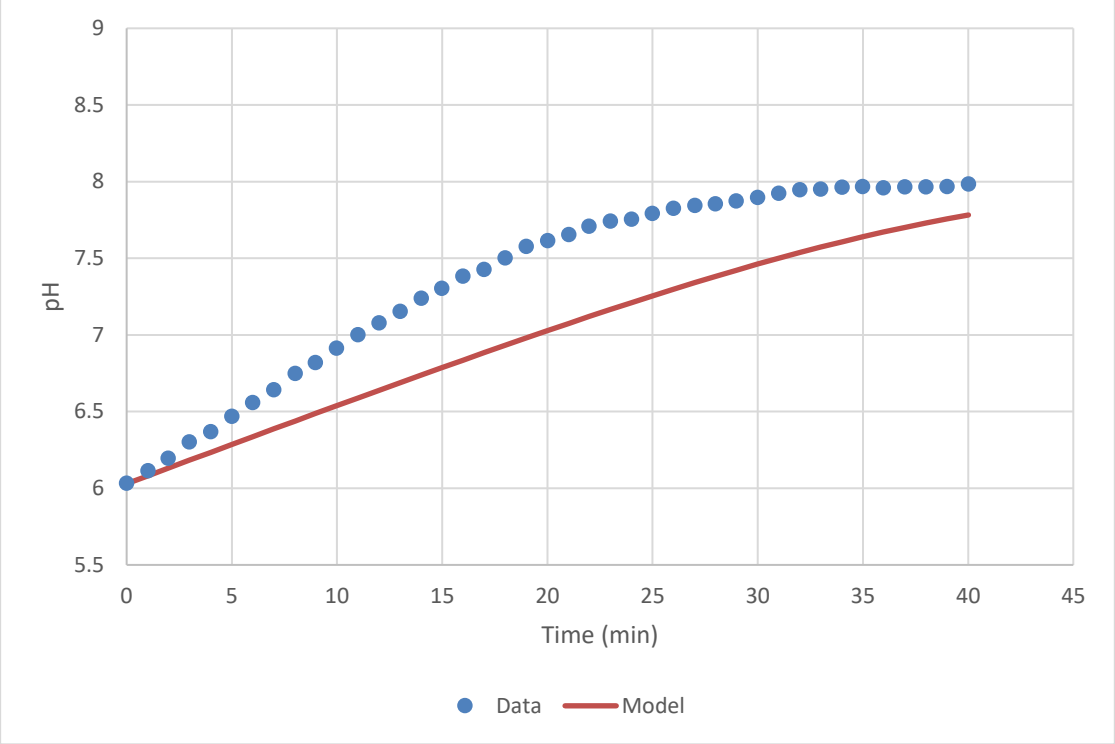

Figure 4.27: pH over time of air in Basic Solution 1, P_{CO_2}=0.000483 atm, $k_c a$=0.119 min^{-1}

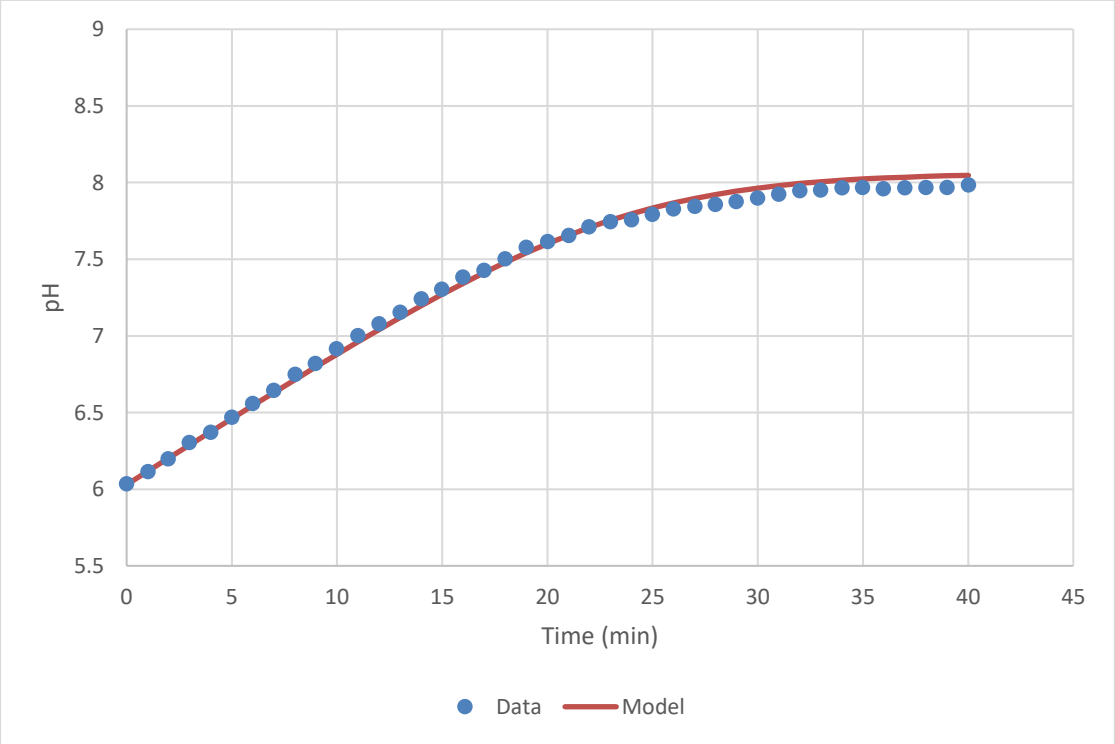

Figure 4.28: pH over time of air Refit in Basic Solution 1, P_{CO_2}=0.000483 atm, $k_c a$=0.202 min^{-1}

It is worth noting that Basic Solution 1 was prepared by using 3 mL of a 1M NaOH solution. This should have given a higher charge than was shown by the data. It is unclear why this charge was so different in the model than what was mixed in the solution. One hypothesis was that the stock solution used was too old and not mixed well. This led to the creation of Basic Solution 2 using a fresh 1M NaOH stock solution. Basic Solution 2 was prepared by using 5 mL of the fresh 1M NaOH solution. This should have given a higher charge than was shown by the data. It is unclear why this charge was so different in the model than what was mixed in the solution. The actual and anticipated charge concentrations in these solutions is shown in Table 4.7. Both solutions were 2 L in total.

Table 4.7 – Differences in Charges of Basic Solutions

Run	**Stock Molarity**	**mL Stock Added**	**Expected [+] (mol/L)**	**Experimental [+] (mol/L)**	**% Error**
Basic Solution 1	1M	3	0.0015	8.47×10^{-4}	43.5%
Basic Solution 2	1.006M	5	0.0030	6.99×10^{-4}	76.7%

The same experiments were run in Basic Solution 2 as in Basic Solution 1. The same values for P_{CO_2} were used for 5% CO_2 and air. The only difference was the charge, both expected and actual. The data and the fitted models are shown in Figures 4.29 and 4.30. Again, the optimal $k_c a$ values did not align. This is why the air run was refit in Figure 4.31. The model variables for both solutions are given in Table 4.8.

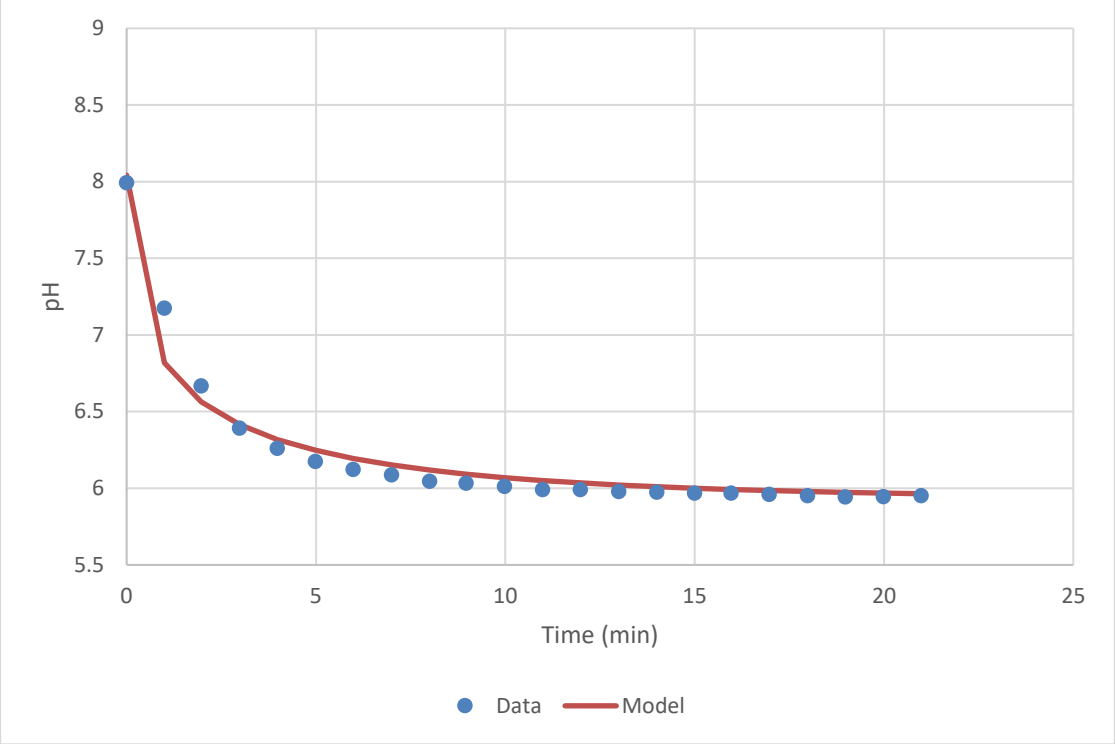

Figure 4.29: pH over time of 5% CO_2 in Basic Solution 2, P_{CO_2}=0.0536 atm, $k_c a$=0.133 min^{-1}

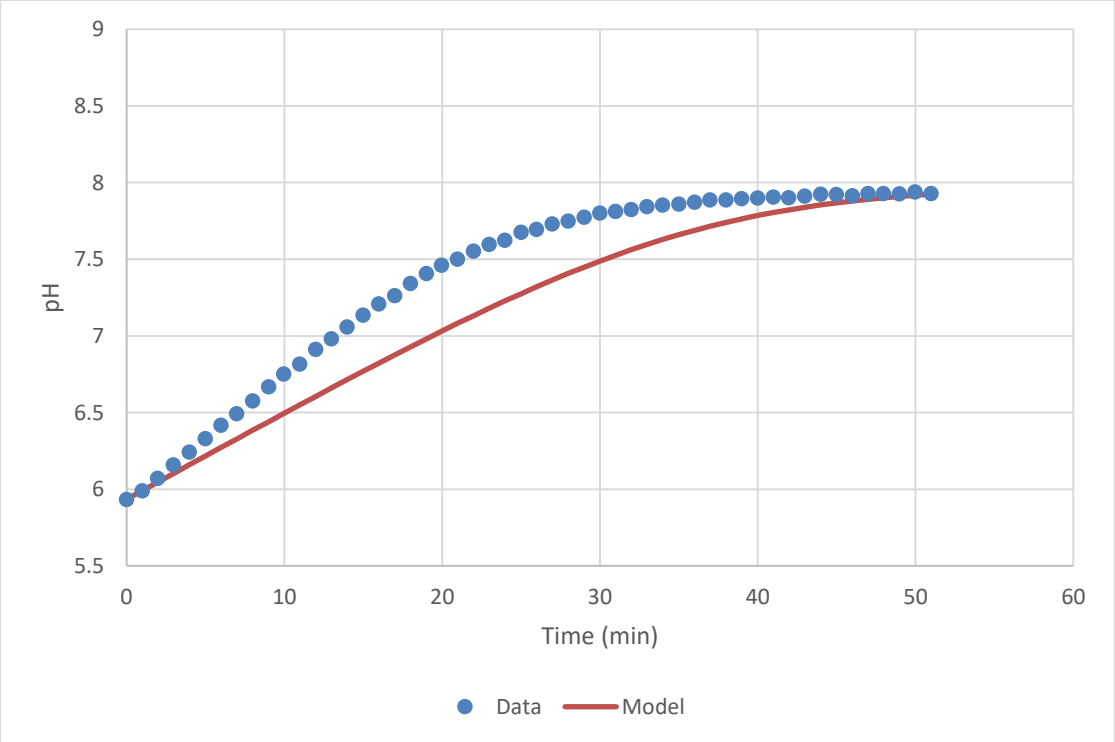

Figure 4.30: pH over time of air in Basic Solution 2, P_{CO_2}=0.000483 atm, $k_c a$=0.133 min^{-1}

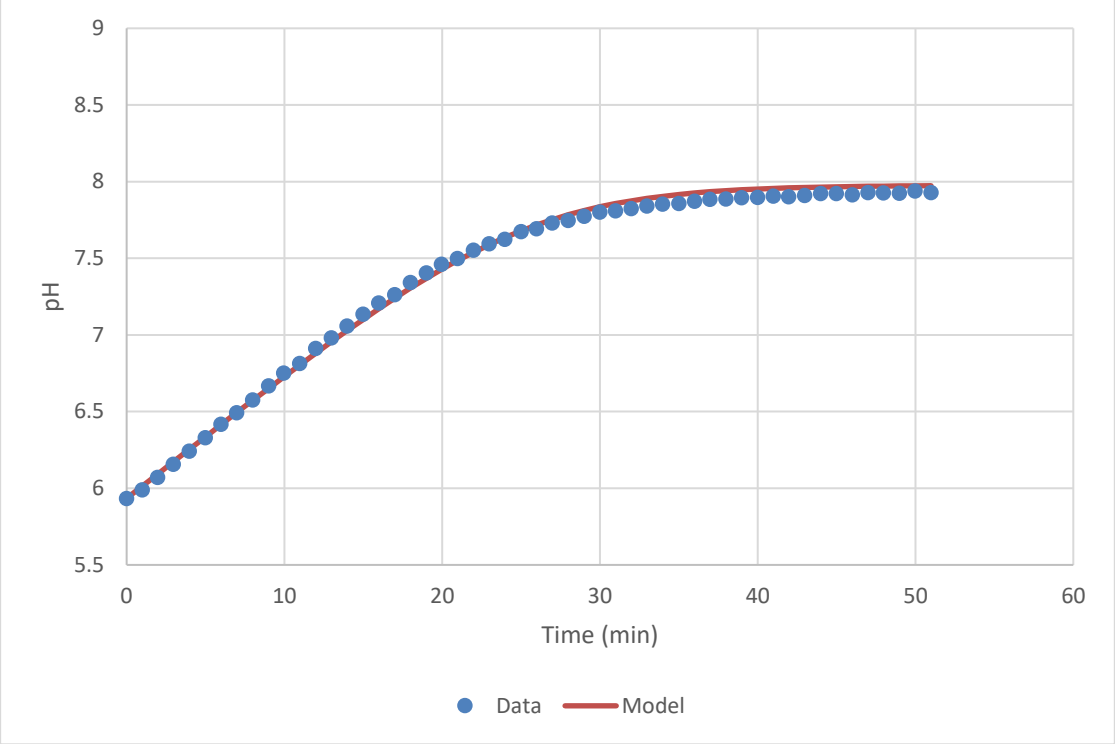

Figure 4.30: pH over time of air Refit in Basic Solution 2, P_{CO_2}=0.000483 atm, k_ca=0.189 min^{-1}

Table 4.8 – Results for Experiments in Basic Solutions

Run	**c_{T0} (mol/L)**	**P_{CO_2} (atm)**	**k_ca (min^{-1})**	**r^2**
Basic Solution 1 Air	2.619 x 10^{-3}	0.000483	0.119	0.547
Basic Solution 1 Air Refit	2.619 x 10^{-3}	0.000483	0.202	0.995
Basic Solution 1 5%	8.586 x 10^{-4}	0.0536	0.119	0.922
Basic Solution 2 Air	2.527 x 10^{-4}	0.000483	0.133	0.830
Basic Solution 2 Air Refit	2.527 x 10^{-4}	0.000483	0.189	0.997
Basic Solution 2 5%	7.105 x 10^{-4}	0.0536	0.133	0.964

As shown in Table 4.8, the k_ca obtained in the absorption process in Basic Solution 2 fit the desorption process better than the Basic Solution 1 counterparts. Overall, the optimal constants were

similar between the two basic solutions for both the 5% and air trials. The air seemed to be faster in both solutions, which is opposite of what was observed in the PECOS media seen in Table 4.4.

These experiments show that pH can be accurately modeled by this method. The range of volumetric convective mass transfer coefficients obtained in this experiment is generally slightly lower than the expected range from previous studies [12]. It is unclear why this is. It was also found that the found convective mass transfer coefficient cannot always be applied to both CO_2 absorption and desorption. This suggests that there is likely a difference in bubble size between the air and CO_2 feeds. This may be due to differences in feed line pressures, or that the BioFlo pushes the gases out at slightly different rates.

5. Conclusion:

The algal growth experiments showed the role of CO_2 in the growth of *Chlorella sorokiniana*. The growth was modeled with a one parameter Verhulst kinetics fit. These results supported the hypothesis that an excess of CO_2 fed into the system would not greatly affect the growth of the algae. The results show that CO_2 content in the gas fed to the reactor greater or equal to 0.8% did not affect growth, while 0.3% content resulted in a slower growth rate and lower final algae concentration. Somewhere between these values, CO_2 becomes the limiting reactant. To further this aspect of the study, it is required to do more trials of algal growth between these two values to find a more accurate value where CO_2 becomes limiting.

The dynamic pH modeling experiments showed that the pH in an aqueous system bubbling CO_2 can be accurately modeled through the proposed equations. This model made use of a one parameter equation based on convective volumetric mass transfer to fit the data. The results of the experiments showed that the actual and nominal amounts of CO_2 in both air and the 0.3% CO_2 from the BioFlo system were not the actual values. This made sense for air because the house air at the University of Arizona likely has a greater composition of CO_2 than the global average. The 0.3% CO_2 from the BioFlo was likely inaccurate due to machine tolerance errors. The experiments also show that the convective mass transfer coefficients for the CO_2 adsorption and desorption processes are likely different from each other. This goes against the hypothesis that they are the same. Additionally, the model reported a much lower concentration of sodium ions than was expected in both NaOH solutions. Further studies can be done to assess why the differences in convective mass transfer coefficients and sodium ion concentrations occur.

6. Appendices:

6.1 Appendix A – Carbon Dioxide Model Formulation

Modeling CO_2 dynamics during algae growth

Dr. Avelino Eduardo Saez

CO_2 system equilibrium

The dissolution of CO_2 in aqueous media leads to two nonionic species: $CO_{2(aq)}$ and H_2CO_3. The latter is formed after dissolution by the reaction

$$CO_{2(aq)} + H_2O \rightleftharpoons H_2CO_3 \quad (1)$$

It is customary to represent both species as a pseudo-species $H_2CO_3^*$, so that

$$[H_2CO_3^*] = [H_2CO_3] + [CO_{2(aq)}] \quad (2)$$

However, H_2CO_3 is usually present in negligible concentrations. The dissolution equilibrium is represented by Henry's law,

$$[H_2CO_3^*] = K_H P_{CO_2} \quad (3)$$

where P_{CO_2} is the partial pressure of CO_2 in the gas phase and K_H is Henry's law constant, which is a function of temperature. The equilibrium reactions of relevance in the liquid are

$$H_2CO_3^* \rightleftharpoons H^+ + HCO_3^- \qquad K_{a1} \quad (4)$$

$$HCO_3^- \rightleftharpoons H^+ + CO_3^= \qquad K_{a2} \quad (5)$$

The equilibrium relations are

$$K_{a1} = \frac{[H^+][HCO_3^-]}{[H_2CO_3^*]} \quad (6)$$

$$K_{a2} = \frac{[H^+][CO_3^=]}{[HCO_3^-]} \quad (7)$$

The basis for the equilibrium calculation of species in an open system is the charge balance. If CO_2 is the only species present in water, the charge balance is

$$[H^+] = [HCO_3^-] + 2[CO_3^=] + [OH^-] \quad (8)$$

The dissociation constant for water is

$$H_2O \rightleftharpoons H^+ + OH^- \qquad K_w \quad (9)$$

$$K_w = [H^+][OH^-] \quad (10)$$

From equations (3) and (6), we have

$$[HCO_3^-] = \frac{K_{a1}[H_2CO_3^*]}{[H^+]} = \frac{K_{a1}K_H P_{CO_2}}{[H^+]} \quad (11)$$

From equations (7) and (11) we get

$$[CO_3^=] = \frac{K_{a2}[HCO_3^-]}{[H^+]} = \frac{K_{a1}K_{a2}K_H P_{CO_2}}{[H^+]^2} \quad (12)$$

Substituting equations (10), (11) and (12) into equation (8) leads to

$$[H^+] = \frac{K_{a1}K_H P_{CO_2}}{[H^+]} + 2\frac{K_{a1}K_{a2}K_H P_{CO_2}}{[H^+]^2} + \frac{K_w}{[H^+]} \quad (13)$$

Given a partial pressure of CO_2 in the gas, this equation can be solved to calculate $[H^+]$ and then the concentration of all species can be calculated.

Now consider that sodium carbonate, Na_2CO_3, is added to the system. The carbonate ion will dissolved and

be subjected to the equilibrium system above, but the sodium ions will provide additional positive charges in a concentration [+] = 2[Na_2CO_3]. The charge balance (8) and consequently equation (13) will change to

$$[+] + [H^+] = \frac{K_{a1} K_H P_{CO_2}}{[H^+]} + 2\frac{K_{a1} K_{a2} K_H P_{CO_2}}{[H^+]^2} + \frac{K_w}{[H^+]} \quad (14)$$

Prediction of equilibrium pH

An experiment was conducted by filling the reactor with a Pecos growth medium solution at 24 °C and bubbling air until the pH reached an equilibrium value. Subsequently, the gas input was changed to 0.3% CO_2 in air at t = 10 min. After a new equilibrium was reached, the input gas was turned back to air at t = 95 min. The results are shown in Figure 1, along with the predictions of the equilibrium pHs calculated from the equations presented above. Parameters used in the calculations are

The Pecos solution contains 20 mg/L of Na_2CO_3 which gives [+] = 2 [Na^+] = 3.77 × 10^{-4} M

Air: P_{CO2} = 0.0427% (427 ppm)

Air + 0.3% CO_2: P_{CO2} = 0.3427%

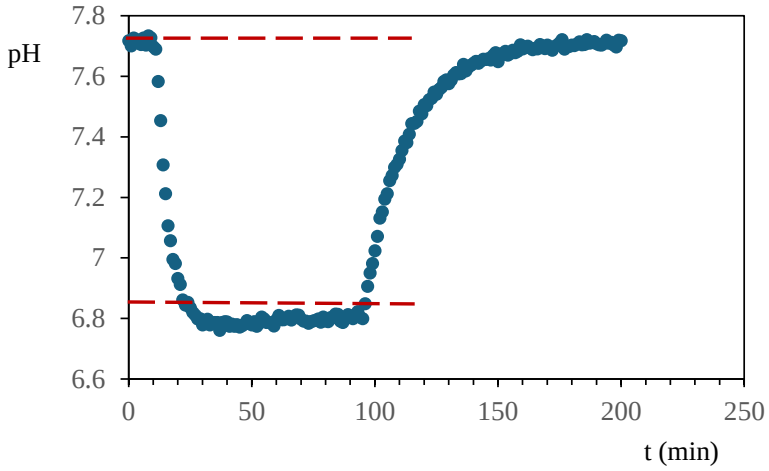

Figure 1. Experimental data (dots) and predictions (dashed lines) of the equilibrium model for Pecos solution equilibrated with air (pH predicted = 7.70) and 0.3% CO_2 in air (pH predicted = 6.84)

CO_2 dissolution kinetics

Experimental data indicates that equilibrium in the open CO_2 system after introducing a change of the gas CO_2 concentration is achieved in the order of minutes. The kinetics of the reactions in the previous sections are associated with times that are many orders of magnitude higher. We conclude that the slow step in the dissolution process is mass transfer from the gas bubbles to the liquid. The convective mass transfer flux from the bubbles to the bulk of the liquid can be written in terms of a mass transfer coefficient as follows,

$$J = k_c([H_2CO_3^*]_i - [H_2CO_3^*]) \tag{15}$$

where J represents moles transferred per unit time and per unit surface area of interface and $[H_2CO_3^*]_i$ is the interfacial concentration of dissolved CO_2. Since this concentration is at equilibrium with the gas, it is represented by equation (3),

$$J = k_c(K_H P_{CO_2} - [H_2CO_3^*]) \tag{16}$$

An instantaneous mole balance of CO_2 in the liquid is

$$V\frac{dc_T}{dt} = AJ = Ak_c(K_H P_{CO_2} - [H_2CO_3^*]) \tag{17}$$

where c_T is the total CO_2 concentration in the liquid, V is the liquid volume and A is the surface area of bubbles. Equation (17) can be written as

$$\frac{dc_T}{dt} = k_c a(K_H P_{CO_2} - [H_2CO_3^*]) \tag{18}$$

where a is the specific surface area of bubbles. Note that $k_c a$ is a volumetric mass transfer coefficient. The total concentration of CO_2 in the liquid is

$$c_T = [H_2CO_3^*] + [HCO_3^-] + [CO_3^=] \tag{19}$$

7. References:

1) Yoro, K. O., & Daramola, M. O. (2020). CO2 emission sources, greenhouse gases, and the global warming effect. In Advances in Carbon Capture (pp. 3–28). Elsevier. https://doi.org/10.1016/b978-0-12-819657-1.00001-3

2) Kane, S., Reilly, J., & Tobey, J. (1992). An empirical study of the economic effects of climate change on world agriculture. In Climatic Change (Vol. 21, Issue 1, pp. 17–35). Springer Science and Business Media LLC. https://doi.org/10.1007/bf00143251

3) Paul Abishek, M., Patel, J., & Prem Rajan, A. (2014). Algae Oil: A Sustainable Renewable Fuel of Future. In Biotechnology Research International (Vol. 2014, pp. 1–8). Wiley. https://doi.org/10.1155/2014/272814

4) Ceron M, Lane T, Ogden K, Thomas Currin R. (2023). ALBUS: ALGAE-BASED BIOPRODUCTS UTILIZING SORBENT-CAPTURED CO2. In F. Kongoli, M.P. Brzezinska, M.A. Alario-Franco, F. Marquis, M.S. Noufal, E. Palomares, J.M. Poblet, D.M. Guldi, A.A. Popov, A.R. Puente Santiago, B. Raveau, D. G. Rodriguez, S. Stevenson, T. Torres, A. Tressaud, M. de Campos (Eds.), Sustainable Industrial Processing Summit Volume 4 Echegoyen Intl. Symp / Nanomaterials for Future Energy Demands (pp. 73-74). Montreal, Canada: FLOGEN Star Outreach

5) Occhipinti, R., & Boron, W. F. (2015). Mathematical modeling of acid-base physiology. In Progress in Biophysics and Molecular Biology (Vol. 117, Issue 1, pp. 43–58). Elsevier BV. https://doi.org/10.1016/j.pbiomolbio.2015.01.003

6) Hofmann, A. F., Meysman, F. J. R., Soetaert, K., & Middelburg, J. J. (2008). A step-by-step procedure for pH model construction in aquatic systems. In Biogeosciences (Vol. 5, Issue 1, pp. 227–251). Copernicus GmbH. https://doi.org/10.5194/bg-5-227-2008

7) Gustafsson, T. K., Skrifvars, B. O., Sandstroem, K. V., & Waller, K. V. (1995). Modeling of pH for Control. In Industrial & Engineering Chemistry Research (Vol. 34, Issue 3, pp. 820–827). American Chemical Society (ACS). https://doi.org/10.1021/ie00042a014

8) Lazic, S. E., Clarke-Williams, C. J., & Munafò, M. R. (2018). What exactly is 'N' in cell culture and animal experiments? In PLOS Biology (Vol. 16, Issue 4, p. e2005282). Public Library of Science (PLoS). https://doi.org/10.1371/journal.pbio.2005282

9) Stumm, W., & Morgan, J. J. (1996). Aquatic Chemistry: Chemical equilibria and rates in natural waters (3rd ed.). Wiley.

10) Fiveable. (2024). 7.2 Convective mass transfer – Intro to Chemical Engineering. https://library.fiveable.me/introduction-chemical-engineering/unit-7/convective-mass-transfer/study-guide/zW5Ca5zgRv9nOg15

11) Olsen, J. E., Dunnebier, D., Davies, E., Skjetne, P., & Morud, J. (2017). Mass transfer between bubbles and seawater. In Chemical Engineering Science (Vol. 161, pp. 308–315). Elsevier BV. https://doi.org/10.1016/j.ces.2016.12.047

12) Hazare, S. R., Vala, S. V., Patil, C. S., Joshi, A. J., Joshi, J. B., Vitankar, V. S., & Patwardhan, A. W. (2022). Correlating Interfacial Area and Volumetric Mass Transfer Coefficient in Bubble Column with the Help of Machine Learning Methods. In Industrial & Engineering Chemistry Research (Vol. 62, Issue 5, pp. 2104–2123). American Chemical Society (ACS). https://doi.org/10.1021/acs.iecr.2c02820

13) Libretexts. (2023). How does a buffer maintain ph?. Chemistry LibreTexts. https://chem.libretexts.org/Bookshelves/Physical_and_Theoretical_Chemistry_Textbook_Maps/Supplemental_Modules_(Physical_and_Theoretical_Chemistry)/Acids_and_Bases/Buffers/How_Does_A_Buffer_Maintain_Ph

14) Ring, T., & Kellum, J. A. (2019). Modeling Acid–Base by Minimizing Charge-Balance. In ACS Omega (Vol. 4, Issue 4, pp. 6521–6529). American Chemical Society (ACS). https://doi.org/10.1021/acsomega.9b00270

15) Powers, E. B. (1930). The Relation between pH and Aquatic Animals. In The American Naturalist (Vol. 64, Issue 693, pp. 342–366). University of Chicago Press. https://doi.org/10.1086/280321

16) 5 things you need to know about algae. Energy.gov. (2017). https://www.energy.gov/eere/articles/5-things-you-need-know-about-algae

17) Blair, M. F., Kokabian, B., & Gude, V. G. (2014). Light and growth medium effect on Chlorella vulgaris biomass production. In Journal of Environmental Chemical Engineering (Vol. 2, Issue 1, pp. 665–674). Elsevier BV. https://doi.org/10.1016/j.jece.2013.11.005

18) Pinto, Crecilla. (2018) Characterization of Dark Cycle of Chlorella Sorokiniana

19) Huesemann, M. H., Van Wagenen, J., Miller, T., Chavis, A., Hobbs, S., & Crowe, B. (2013). A screening model to predict microalgae biomass growth in photobioreactors and raceway ponds. In Biotechnology and Bioengineering (Vol. 110, Issue 6, pp. 1583–1594). Wiley. https://doi.org/10.1002/bit.24814

20) Qiu, R., Gao, S., Lopez, P. A., & Ogden, K. L. (2017). Effects of pH on cell growth, lipid production and CO2 addition of microalgae Chlorella sorokiniana. In Algal Research (Vol. 28, pp. 192–199). Elsevier BV. https://doi.org/10.1016/j.algal.2017.11.004

21) Chu, S. P. (1942). The Influence of the Mineral Composition of the Medium on the Growth of Planktonic Algae: Part I. Methods and Culture Media. In The Journal of Ecology (Vol. 30, Issue 2, p. 284). JSTOR. https://doi.org/10.2307/2256574

22) Cassidy, K. O. (2011). Evaluating algal growth at different temperatures (Master's thesis, University of Kentucky). UKnowledge. https://uknowledge.uky.edu/bae_etds/3

23) Singh, S. P., & Singh, P. (2014). Effect of CO2 concentration on algal growth: A review. In Renewable and Sustainable Energy Reviews (Vol. 38, pp. 172–179). Elsevier BV. https://doi.org/10.1016/j.rser.2014.05.043

24) Parker, W. S. (2020). Model Evaluation: An Adequacy-for-Purpose View. Philosophy of Science, 87(3), 457–477. doi:10.1086/708691

25) Hannon, M., Gimpel, J., Tran, M., Rasala, B., & Mayfield, S. (2010). Biofuels from algae: challenges and potential. In Biofuels (Vol. 1, Issue 5, pp. 763–784). Informa UK Limited. https://doi.org/10.4155/bfs.10.44

26) Lee, E., Jalalizadeh, M., & Zhang, Q. (2015). Growth kinetic models for microalgae cultivation: A review. In Algal Research (Vol. 12, pp. 497–512). Elsevier BV. https://doi.org/10.1016/j.algal.2015.10.004

27) Wu, J. Y., Tso, R., Teo, H. S., & Haldar, S. (2023). The utility of algae as sources of high value nutritional ingredients, particularly for alternative/complementary proteins to improve human health. In Frontiers in Nutrition (Vol. 10). Frontiers Media SA. https://doi.org/10.3389/fnut.2023.1277343

28) Dai, N., Wang, Q., Xu, B., & Chen, H. (2022). Remarkable Natural Biological Resource of Algae for Medical Applications. In Frontiers in Marine Science (Vol. 9). Frontiers Media SA.

https://doi.org/10.3389/fmars.2022.912924

29) Abdel-Raouf, N., Al-Homaidan, A. A., & Ibraheem, I. B. M. (2012). Microalgae and wastewater treatment. In Saudi Journal of Biological Sciences (Vol. 19, Issue 3, pp. 257–275). Elsevier BV. https://doi.org/10.1016/j.sjbs.2012.04.005

30) Lotfigolsefidi, F., Davoudi, M., Sarkhosh, M., & Bonyadi, Z. (2025). Removal of microplastics by algal biomass from aqueous solutions: performance, optimization, and modeling. In Scientific Reports (Vol. 15, Issue 1). Springer Science and Business Media LLC. https://doi.org/10.1038/s41598-024-84114-8

31) Li, Y., Tao, L., Wang, Q., Wang, F., Li, G., & Song, M. (2023). Potential Health Impact of Microplastics: A Review of Environmental Distribution, Human Exposure, and Toxic Effects. In Environment & Health (Vol. 1, Issue 4, pp. 249–257). American Chemical Society (ACS). https://doi.org/10.1021/envhealth.3c00052

32) Georgiou, D., Charisis, A., Theocharidou, A., Ritzoulis, C., Papapanagiotou, G., Samara, C., Chatzidoukas, C., & Kalogianni, E. P. (2024). Foaming Properties of Chlorella sorokiniana Microalgal Biomass. In Colloids and Interfaces (Vol. 8, Issue 6, p. 66). MDPI AG. https://doi.org/10.3390/colloids8060066

33) Shihira, I., & Krauss, R. W. (1965). Chlorella: physiology and taxonomy of forty-one isolates. University of Maryland.

34) Cazzaniga, S., Dall'Osto, L., Szaub, J., Scibilia, L., Ballottari, M., Purton, S., & Bassi, R. (2014). Domestication of the green alga Chlorella sorokiniana: reduction of antenna size improves light-use efficiency in a photobioreactor. In Biotechnology for Biofuels (Vol. 7, Issue 1). Springer Science and Business Media LLC. https://doi.org/10.1186/s13068-014-0157-z

35) New Brunswick bioflo 115 Benchtop Fermentor & Bioreactor: GMI - Trusted Laboratory Solutions. GMI. (2022). https://www.gmi-inc.com/product/new-brunswick-bioflo-115-benchtop-fermentor-bioreactor/?srsltid=AfmBOop6veX_SZ7AVY2oNAeMqnq8DdOVWBi2ZomLW6zoZ6sp9lbb-iJO

36) Held, P. (2021). Monitoring of algal growth using their intrinsic properties. Application Note.

https://www.agilent.com/cs/library/applications/monitoring-of-algal-growth-5994-3290EN-agilent.pdf

37) Shirsat, N., Mohd, A., Whelan, J., English, N. J., Glennon, B., & Al-Rubeai, M. (2014). Revisiting Verhulst and Monod models: analysis of batch and fed-batch cultures. In Cytotechnology (Vol. 67, Issue 3, pp. 515–530). Springer Science and Business Media LLC. https://doi.org/10.1007/s10616-014-9712-5

38) Shimakawa, G., Kohara, A., & Miyake, C. (2020). Characterization of Light-Enhanced Respiration in Cyanobacteria. In International Journal of Molecular Sciences (Vol. 22, Issue 1, p. 342). MDPI AG. https://doi.org/10.3390/ijms22010342

39) Laboratory, N. G. M. (2024). Trends in CO2 - NOAA Global Monitoring Laboratory. GML. https://gml.noaa.gov/ccgg/trends/mlo.html

40) George, K., Ziska, L. H., Bunce, J. A., & Quebedeaux, B. (2007). Elevated atmospheric CO2 concentration and temperature across an urban–rural transect. In Atmospheric Environment (Vol. 41, Issue 35, pp. 7654–7665). Elsevier BV. https://doi.org/10.1016/j.atmosenv.2007.08.018